A new high-resolution Coastal Ice-Ocean Prediction System for the East Coast of Canada

Jean-Philippe Paquin[1] · François Roy[1] · Gregory C. Smith[1] · Sarah MacDermid[2] · Ji Lei[2,3] · Frédéric Dupont[2] · Youyu Lu[4] · Stephanne Taylor[4] · Simon St-Onge-Drouin[5] · Hauke Blanken[6] · Michael Dunphy[6] · Nancy Soontiens[7]

Abstract

The Coastal Ice Ocean Prediction System for the East Coast of Canada (CIOPS-E) was developed and implemented operationally at Environment and Climate Change Canada (ECCC) to support a variety of critical marine applications. These include support for ice services, search and rescue, environmental emergency response and maritime safety. CIOPS-E uses a 1/36° horizontal grid (~2 km) to simulate sea ice and ocean conditions over the northwest Atlantic Ocean and the Gulf of St. Lawrence (GSL). Forcing at lateral open boundaries is taken from ECCC's data assimilative Regional Ice-Ocean Prediction System (RIOPS). A spectral nudging method is applied offshore to keep mesoscale features consistent with RIOPS. Over the continental shelf and GSL, the CIOPS-E solution is free to evolve according to the model dynamics. Overall, CIOPS-E significantly improves the representation of tidal and sub-tidal water levels compared to ECCC's lower resolution systems: RIOPS (~6 km) and the Regional Marine Prediction System – GSL (RMPS-GSL, 5 km). Improvements in the GSL are due to the higher resolution and a better representation of bathymetry, boundary forcing and dynamics in the upper St. Lawrence Estuary. Sea surface temperatures show persistent summertime cold bias, larger in CIOPS-E than in RIOPS, as the latter is constrained by observations. The seasonal cycle of sea ice extent and volume, unconstrained in CIOPS-E, compares well with observational estimates, RIOPS and RMPS-GSL. A greater number of fine-scale features are found in CIOPS-E with narrow leads and more intense ice convergence zones, compared to both RIOPS and RMPS-GSL.

Responsible Editor: Mauro Cirano.

✉ Jean-Philippe Paquin
  jean-philippe.paquin@ec.gc.ca

1 Division de la Recherche en Météorologie, Environnement et changement climatique Canada, Dorval, Canada

2 Service Météorologique du Canada, Environnement et changement climatique Canada, Dorval, Canada

3 Canadian Hydrographic Services, Fisheries and Oceans Canada, Dorval, Canada

4 Bedford Institute of Oceanography, Fisheries and Oceans Canada, Dartmouth, Canada

5 Institut Maurice-Lamontagne, Pêches et Océans Canada, Mont Joli, Canada

6 Institute of Ocean Sciences, Fisheries and Oceans Canada, Victoria, Canada

7 North Atlantic Fisheries Centre, Fisheries and Oceans Canada, St. John's, Canada

1 Introduction

The Coastal Ice-Ocean Prediction System (CIOPS) was recently developed and implemented operationally in 2021 at the Canadian Centre for Meteorological and Environmental Prediction (CCMEP, formerly the Canadian Meteorological Centre), as part of the Government of Canada's Oceans Protection Plan initiative. This high-resolution ice-ocean prediction system is developed with the objectives of (i) increasing the numerical guidance available in the eventuality of marine environmental emergencies and (ii) providing accurate forecasting of water levels and near-surface currents to improve navigational safety in Canadian coastal waters. CIOPS is composed of two separate systems: CIOPS-E, covering the Canadian East Coast from the Gulf of Maine (42°N) to the southern part of the Labrador Shelf (53°N); and CIOPS-W, covering the Canadian West

Coast from 44°N to 61°N. Here we provide a description and detailed evaluation of the CIOPS-E system. A similar evaluation of CIOPS-W is provided in Paquin et al. (2021b, 2022b).

The development of CIOPS is aligned with an increase internationally in the number of coastal ocean forecasting systems using horizontal resolutions on the order of a few kilometres. Such high-resolution is necessary to capture the complex coastal interactions that occur over a broad range of spatial and temporal scales between near-shore dynamics, land hydrology, river discharge and atmospheric forcing (Kourafalou et al. 2015a, b). Examples of such systems include the Copernicus Marine Iberia-Biscay-Ireland System (IBI; Maraldi et al. 2013; Lorente et al. 2019; Garcia Sotillo et al. 2021), the Western Mediterranean Operational System (WMOP; Aguiar et al. 2020) and the US West Coast Ocean Forecast System (WCOFS; Kurapov et al. 2017). Some ocean systems also have versions including data assimilation, such as the Met Office North-West European Shelf forecasting system (Tonani et al. 2019). Sakamoto et al. (2019) and Hirose et al. (2019) developed a data assimilative and operational forecasting model at a similar resolution to capture the processes in the coastal and open-ocean areas around Japan. A coastal downscaling system for the Mediterranean Sea has been developed by combining structured and unstructured ocean models (Trotta et al. 2016, 2017) for similar and higher resolution applications. The CIOPS systems additionally support sub-kilometer port scale modelling systems currently in development at the Canadian Department of Fisheries and Oceans by providing high frequency boundary conditions. CIOPS-E specifically support three port-scale models for: Saint John Harbour in the Bay of Fundy (Paquin et al. 2019), Port of Canso in Nova Scotia and a sub-kilometer modelling system of the St. Lawrence Estuary. The variety of systems developed and implemented internationally also allows for different groups to improve their understanding of model behaviour and limitations via inter-model comparison studies (e.g., Nudds et al. 2020).

At CCMEP, two ice-ocean prediction systems covering the East Coast of Canada have been running operationally, the Regional Ice-Ocean Prediction System (RIOPS; Dupont et al. 2015; Smith et al. 2021) and the Regional Marine Prediction System for the Gulf of St. Lawrence (RMPS-GSL; Pellerin et al. 2004; Smith et al. 2013; Roy et al. 2014).

RIOPS covers all oceans around Canada, from north of 26°N in the Atlantic Ocean, the entire Arctic Ocean, to north of 44°N in the Pacific Ocean. The horizontal grids of RIOPS follow the tri-polar ORCA configuration developed by the DRAKKAR Group (2007) with a nominal resolution of 1/12° in longitude/latitude, around 6 km in oceans off the Canadian East Coast and, can therefore be considered to be eddy permitting over the shelf and coastal areas (Dupont et al. 2015). RIOPS uses a multi-variate reduced-order Kalman filter, assimilating satellite altimetry, temperature, and salinity profiles (e.g., from Argo, field campaigns, moorings, drifting buoys, gliders, etc.), combined with a 3DVar large-scale low-frequency correction to water mass properties. The ocean assimilation is also combined with a 3DVar sea ice analysis (Buehner et al. 2013, 2016). RIOPS has been shown to provide an adequate constraint on mesoscale features in the Gulf Stream region (Smith et al. 2021).

The RMPS-GSL is an operational ice-ocean prediction system limited to the Gulf of St. Lawrence. The ocean and sea ice components are run on a 5 km horizontal resolution, where only the ocean is constrained through open boundaries. Tides are explicitly resolved with elevation and transport provided at the two boundary conditions of Cabot and Belle-Isle Straits (Fig. 1). The RMPS-GSL uses monthly climatological boundary conditions of the three-dimensional temperature and salinity at both straits. The effect of atmospheric pressure on the ocean's surface (inverse barometer) is not considered in the RMPS-GSL. The RMPS-GSL boundary conditions do not include time-varying residual (non-tidal) water level, therefore the storm surge signal generated over the North Atlantic cannot propagate into the model domain, greatly limiting the representation of the water level accuracy in the GSL. The RMPS-GSL was used to initialize a daily 48 h coupled atmosphere-ice-ocean forecast with a 10 km resolution atmospheric domain.

CIOPS-E was developed in order to achieve higher accuracy in the representation of the tidal and non-tidal water levels over the coastal areas compared to RIOPS, whilst also expanding and enhancing the high-resolution coverage of RMPS-GSL over the Canadian coastal waters. By combining the higher resolution over the shelf and the large-scale constraints offshore via a spectral nudging method, CIOPS-E aims to better represent the fine-scale structures on the shelf and interactions with the energetic mesoscale variability (eddies and meanders) in the Gulf Stream-North Atlantic Current system. Here we demonstrate the extent to which CIOPS-E achieves these goals and thus can be used to improve numerical guidance applied to environmental response and navigational safety in the coastal environment.

This paper presents a detailed description of the CIOPS-E model configuration and spectral nudging method in Sect. 2. Section 3 presents a thorough evaluation against observations and ECCC's operational systems (RIOPS and RMPS-GSL). The evaluation is focused on variables influencing the representation of near-surface currents and water mass properties crucial to the emergency response capabilities: tidal amplitudes and phases, sub-tidal water levels, sea surface temperatures, vertical profiles of temperature and salinity and sea ice cover and thickness. Section 4 concludes

by presenting a summary of CIOPS-E improvements over the pre-existing systems, its current limitations, and suggestions for future improvements.

2 CIOPS-E system description

CIOPS-E is composed of two main components, a "pseudo-analysis" that provides a continuous simulation and a forecast component that provides 48 h forecast four times per day. Here we consider only the pseudo-analysis component and leave the forecast component as the focus of a subsequent study. This section presents details of CIOPS-E, including the ocean and sea ice models, along with the system's operational configuration. Details are provided regarding the computational domain and bathymetry, ocean and tidal boundary conditions, river discharge and atmospheric forcing. The last section describes the spectral nudging method applied to constrain offshore mesoscale variability.

2.1 Ocean-sea ice model

The CIOPS-E modelling system uses the Nucleus for European Modelling of the Ocean version 3.6 (NEMO; Madec et al. 2015) coupled to the Los Alamos Community Ice CodE version 4 (CICE4; Hunke 2001; Lipscomb et al. 2007; Hunke and Lipscomb 2008). The following sections describe both modelling components and parameters, including differences with RIOPS.

2.1.1 Nucleus for European modelling of the ocean (NEMO)

The NEMO ocean model solves the three-dimensional governing equations of ocean circulation and hydrography (temperature and salinity) on a structured computational grid, with the hydrostatic and Boussinesq approximations. The ocean model uses 100 vertical z-levels, with spacing increasing from 1 m at the surface over the first 20 m, to 200 m at 5000 m depth. Bottom partial steps are employed for an accurate representation of the varying bathymetry. The use of "variable volume level" (Levier et al. 2007) allows the thickness of vertical levels to vary with changes in the sea surface elevation.

The momentum advection follows the 3rd order Upstream-Biased Scheme (UBS; Shchepetkin and McWilliams 2005). Along the lateral solid boundaries (coastlines), a partial-slip boundary condition is used to allow the frictional effects of the lateral boundaries to be included without the restrictive resolution required to represent the lateral boundary layer under no-slip conditions. Tracers are advected using the Total Variance Dissipation (TVD) scheme in both horizontal and vertical directions (Madec

et al. 2015). A vertical split-explicit time stepping with five sub-timesteps is used to ensure stability. The lateral diffusion on tracers and momentum uses 3D time-varying viscosity following Smagorinsky (1993) in which the viscosity coefficient is proportional to a local deformation rate based on horizontal shear and tension. A time-splitting scheme is applied for the internal (baroclinic) and external (barotropic) modes. The time step for the internal (external) mode is set to 150 s (5 s). Vertical turbulence and mixing are calculated through the $k-\varepsilon$ configuration of the generic length scale (GLS) turbulence closure (Umlauf and Burchard 2003) with background vertical eddy viscosity and diffusivity set to 1.0×10^{-4} m^2 s^{-1} and 1.0×10^{-5} m^2 s^{-1}, respectively. Sensitivity experiments showed optimized tides in the St. Lawrence Estuary when using the bottom non-linear log-layer formulation with a bottom roughness of 2×10^{-4} m (Paquin et al. 2021a, 2022a). Table 1 summarizes the main CIOPS-E ocean model parameters, alongside those from RIOPS for comparison.

Preliminary experiments revealed a large-scale cold surface temperature bias in summer that was reduced through model physics adjustments. First, the surface turbulent kinetic energy (TKE) input from wave breaking, where the significant wave height (H_s) is based on the Rascle et al. (2008) formula, was reduced by adjusting the multiplication factor used to compute the surface roughness length (z_0). A decrease of the roughness length (from $z_0 = 1.3H_s$ to $z_0 = 0.75H_s$) reduced the surface mixing in summer and hence the cold bias. Second, the ocean surface momentum transfer was adjusted to (i) add a surface wave representation in the wind stress computation (expected to be more realistic in fall and winter) and (ii) to make the wind stress computation consistent with the TKE wave breaking input formulas as noted above. The wave breaking TKE input formulas are based on Rascle et al. (2008) and Mellor and Blumberg (2004) where the relation between sea surface height (roughness) and wind stress is derived from Smith et al. (1992). Therein, the sea surface roughness length (z_{0a}) is derived from the following Charnock-type formula:

$$z_{0a} = \alpha \left(\frac{C_p}{u_*} \right)^\beta \frac{u_*^2}{g} \qquad (1)$$

where Cp/u* is the wave age, u* is the friction velocity, g is the acceleration due to gravitation, and $\alpha = 0.45$ and $\beta = -1$ are tuneable parameters. Using this same formula instead of the one from Large and Yeager (2004) for the Common Ocean-ice Reference Experiments (CORE) makes the surface wind stress consistent with the TKE wave breaking input formula. The consequence is to have more surface mixing in fall and winter but slightly less in summer (for winds below 5 m s^{-1}). Finally, increased vertical mixing in

Table 1 Main ocean model parameters

Parameter	RIOPS	CIOPS-E
NEMO version	3.6	3.6
Time step	300s (barotropic 5s)	150s (barotropic 5s)
Vertical levels	75	100
Momentum advection	3rd order ubs	3rd order ubs
BDY Barotropic	Flather	Flather
BDY Baroclinic dyn	Specified	Specified
BDY tracer	Specified	Specified
Lateral diff. momentum	Lap. (50m2/s)	Bilaplacian + smagorinsky
Lateral mom. cond.	Free slip	Partial slip (shlat = 1.0)
Lateral diff. tracers	Bilap.	Laplacian + smagorinsky
Bottom friction	Non-linear / loglayer	Non-linear / loglayer
Vertical diffusion	k-ε (GLS)	k-ε (GLS)
Solar penetration	2-band	2-band
Large-scale "correction"	Data assimilation	Spectral nudging
Ocean boundary data	GIOPS	RIOPS-F
Tides	OSU / FES (13)	OSU / FES (13)
Atmospheric forcing	Blended GDPS – RDPS	Blended GDPS – HRDPS
Atm. forcing resolution	15 km–10 km	15 km–2.5 km
Forcing frequency	3 h	1 h
Atmospheric pressure	Yes	Yes
River runoff	Dai&Trenberth + 1D St Laurent	Dai&Trenberth, Saucier et al. (2003) & 1D St Laurent

the upper St. Lawrence Estuary is introduced to stimulate the estuarine circulation as the model resolution is not sufficient to resolve the mixing processes there related to the interaction of the high runoff from the St. Lawrence River with rugged topography and strong tides (Saucier and Chassé 2000). We artificially increase the surface wind stress by 50% and vertical mixing coefficients (increase of 2×10^{-2} m^2 s^{-1}) west of Tadoussac (see Fig. 1). Impact studies for individual changes are presented in Paquin et al. (2021a).

2.1.2 Los Alamos Community Ice CodE (CICE)

The sea ice model CICE is used to represents the sea ice dynamics using an elastic-viscous plastic rheology and the sea ice thermodynamics using Bitz and Lipscomb (1999) parameterization over ten ice thickness categories, three ice vertical layers and a single snow layer. We use the seabed stress approach to parameterize landfast ice following Lemieux et al. (2015, 2016). The model parameters are consistent with RIOPS (Dupont et al. 2015). The ice-ocean drag

coefficient is computed by a log-layer assumption following Roy et al. (2015). The ice strength parameters P* and C* are 27.5 kN m^{-2} and 20 respectively. No sea ice open boundary conditions are provided at the northern boundary and therefore the sea ice advected from the Labrador Shelf is neglected. The impact of this limitation is discussed later in this paper, and we note that the next version of the CIOPS-E system will include the Labrador Shelf ice flux.

2.2 CIOPS-E operational configuration

This section describes the operational implementation of the CIOPS-E system, including the model domain and bathymetry, the ocean open and tidal boundary conditions, the freshwater river discharge and the atmospheric forcing.

2.2.1 Model domain and bathymetry

The CIOPS-E model domain (Fig. 1) follows the ORCA tripolar grid projection (Madec and Imbard 1996) and covers the Northwest Atlantic Ocean at a nominal 1/36° horizontal resolution, corresponding to an average grid spacing of about 2 km. The model covers the area from Cape Hatteras (~35°N) to the southern part of Labrador (~54°N), from the coast to 35°W. Hence the model incorporates key areas such as the Gulf Stream separation region, the Grand Banks of Newfoundland, the Gulf of St. Lawrence, the Scotian Shelf and the Bay of Fundy.

The reference bathymetric dataset for the deep ocean is interpolated from the global dataset of Smith and Sandwell (SRTM30_plus version 11; Becker et al. 2009). Over the Scotian Shelf, the Gulf of Maine and the Bay of Fundy, the bathymetry field is re-interpolated from the high-resolution data used in the Gulf of Maine – Scotian Shelf model (GoMSS; Katavouta et al. 2016). Over the GSL, the background bathymetry information is further refined with additional sounding information collected by the Canadian Department of Fisheries and Oceans (DFO). Due to the presence of the world's largest tidal range, reaching 16 m in the upper Bay of Fundy, and because NEMO version 3.6 does not include a wetting-drying scheme, a minimum depth of 7.5 m is imposed over the model domain to ensure no ocean point would dry out. The area around and in Minas Basin at the upmost region of the Bay of Fundy was also deepened and the geometry of the basin was changed accordingly to conserve the total volume. This ensures numerical stability while conserving tidal resonance, allowing for realistic tides in the region. The limitations due to the minimum depth and geometry changes will be removed in future CIOPS-E versions, using the wetting-drying scheme from updated NEMO versions.
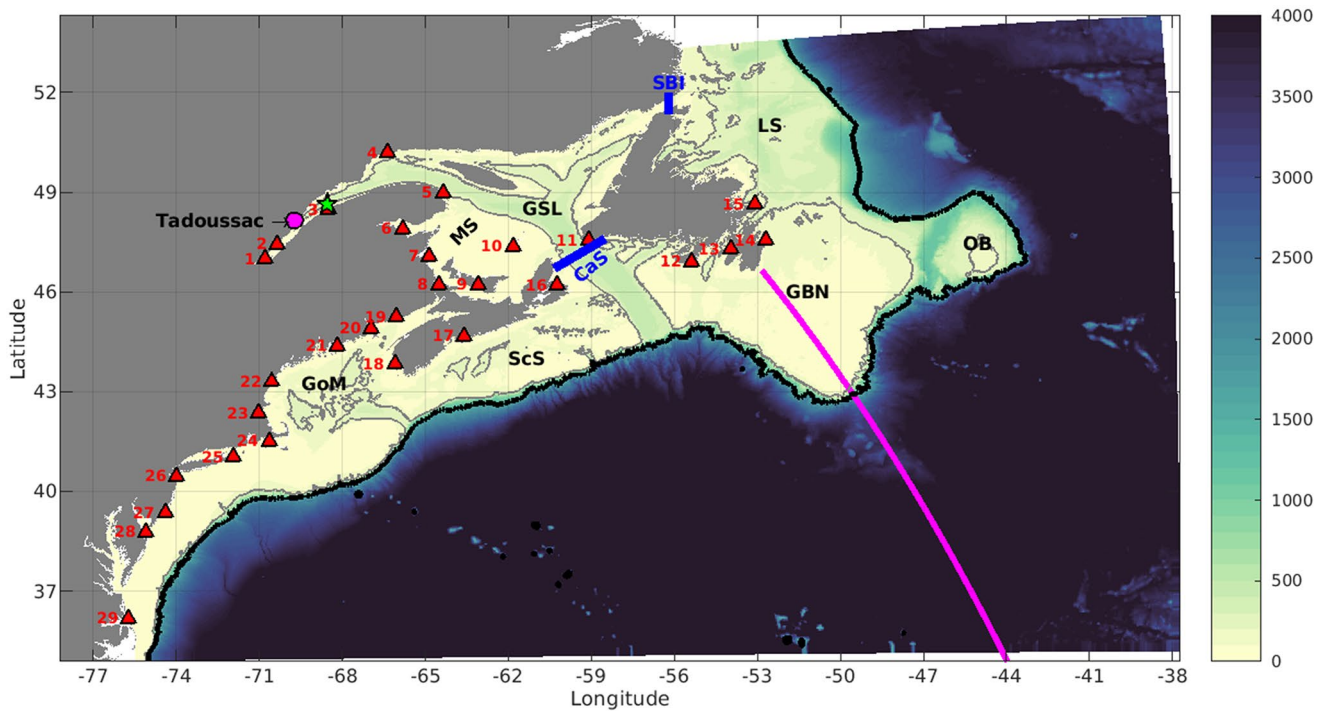
Fig. 1 Bathymetry (m, colours) of the CIOPS-E domain. The grey and black contours show the 200 m and 1500 m isobaths, respectively. Red triangles show the coastal tide gauges referenced in the text and in Table 2. The location of IML-4 buoy and Tadoussac are identified by the green star and magenta circle, respectively. The Jason 2 altimeter track #226 (referenced in Fig. 2) is presented as the bold magenta line. Geographic areas are abbreviated in black for the Gulf of Maine (GoM), Scotian Shelf (ScS), Grand Banks of Newfoundland (GBN), Orphan Basin (OB), Labrador Shelf (LS), the Gulf of St. Lawrence (GSL), and the shallow area in the southwest part of the GSL is identified as the Magdalen Shallows (MS). The two straits enclosing the GSL are identified by the blue lines: Belle Isle Strait (BIS) and Cabot Strait (CaS)

2.2.2 Ocean open boundary conditions

The ocean model is forced at its open boundaries with sea surface height (SSH) and three-dimensional temperature, salinity and velocity fields from RIOPS (Smith et al. 2021). Hourly SSH from RIOPS is de-tided using the ECCC online harmonic analysis tool (described in Smith et al. 2021) before daily averages are computed. The three-dimensional temperature, salinity and velocities are daily averaged. Some residual tidal energy is still present but was not identified as an obvious source of errors. Linear interpolation is used between daily averaged values, which is especially important for the SSH to avoid creating shocks at date change that would otherwise generate spurious gravity waves.

Tidal forcing is imposed at the lateral boundaries using elevation and barotropic transports of 13 constituents (M2, S2, N2, K2, K1, O1, P1, Q1, Mf, Mm, M4, MS4 and MN4) from the Oregon State University TPXO tidal model (Egbert and Erofeeva 2002), hereafter referenced as OSU. Note that the overtides (M4, MS4 and MN4) are mainly generated by the nonlinear dynamics inside the model domain, and are less caused by the open boundary forcing. Here the TPXO solution is used for the tidal OBC because it is more

accurate than the tidal solution of RIOPS. The prescribed self-attraction and loading terms are interpolated from the Finite Element Solution (FES 2012) tidal product (Carrère et al. 2012). The radiation scheme of Flather (1976) is applied to obtain the barotropic current normal to the lateral open boundaries. This method adjusts the input of barotropic transport according to the difference between the model-calculated and input SSH, and allows the numerical noise generated inside the model domain to easily propagate outside. The inputs of both barotropic transport and SSH are the sum of non-tidal and tidal components. This approach has been shown in other studies to provide more accurate tidal forcing and reduced aliasing of the tidal signal (Janekovic and Powell (2011).

2.2.3 River runoffs and the St. Lawrence 1D model

The freshwater discharge from rivers flowing in the CIOPS-E domain are derived from climatological data, except for the St. Lawrence River. For the GSL, a monthly runoff climatology based on observations from the 28 most important tributaries is used (Saucier et al. 2003). Outside the GSL, data from Dai and Trenberth (2002) are used to compute the runoff climatology.

The monthly climatology is further interpreted to daily values and applied to the ocean model as a surface volume flux (similarly to precipitation) at the ocean model point closest to the river outlet. The freshwater discharge is assumed to be at the same temperature as the ocean surface temperature, except for the St. Lawrence River, where a monthly climatology of temperature recorded near Québec City is used.

The St. Lawrence River is the largest source of freshwater over the model domain, with an mean discharge of 11×10^3 m^3 s^{-1} (11 mSv) and a spring freshet that often exceeds 20×10^3 m^3 s^{-1} (20 mSv) (Bourgault and Koutitonsky 1999). The ocean model domain reaches the vicinity of Québec City (Fig. 1) where the water level is still influenced by tides. To alleviate complexities of both the freshwater flux and to absorb the energy of the incoming tides, CIOPS-E uses a one-dimensional model for the St. Lawrence River (Dronkers 1969). This 1D model has a long history of being coupled to Saucier et al. (2003) model of the GSL and, in fact, the same coupling strategy was ported to CIOPS-E. It is an implicit-in-time finite element 1D model computing the evolving water levels and river discharge at each point. It takes discharge as the upstream boundary condition and water level at the downstream (ocean) boundary condition. It allows for branching and merging of the river. The same one-dimensional model is also used in both RIOPS and RMPS-GSL. The daily freshwater discharge (in m^3 s^{-1}) is obtained from the DFO real-time estimate (Lefaivre et al. 2016).

2.2.4 Atmospheric forcing

The ocean model is forced at its surface by hourly fields from the Canadian Global Environmental Multiscale (GEM) Numerical Weather Prediction Model (Côté et al. 1998). Forcing variables include hourly winds, air temperature and specific humidity at the lowest prognostic level of the atmospheric model (~40 m), precipitation, and surface downward short- and long-wave radiation. Bulk formulas are adjusted to account for the modified reference height. The atmospheric boundary layer parameterization used in NEMO is modified to be consistent with ECCC NWP models. This approach reduces the inconsistencies in the boundary layer physics and limits the influence of the surface (ocean, ice or land) conditions imposed in the atmospheric NWP model as the conditions are further up than the standard 10 m and 2 m heights. Moreover, this approach reduces the potential differences in the coastline (land-sea mask) between the forcing model and the ocean-ice model. Forcing from atmospheric pressure is also included in the ocean momentum equation to represent the inverse barometer effect on the ocean's surface. Two configurations of

the GEM model are combined to cover the entire CIOPS-E domain. The majority of the ocean domain is covered by the High-Resolution Deterministic Prediction System (HRDPS; Milbrandt et al. 2016; Caron 2022) with a grid resolution of 2.5 km. As the southeastern corner of the ocean domain is not covered by the HRDPS, the HRDPS fields are combined with those from the 15-km resolution Global Deterministic Prediction System (GDPS; Gasset 2019). To avoid creating unphysical changes in the atmospheric fields at the junction of the two grids, a spatio-temporal blending technique is used. In brief, from the southeastern limit of the HRDPS grid inward, a weighted average over a transition area of 100 grid points (~250 km) is performed where the GDPS solution is gradually replaced by that from the HRDPS. Both atmospheric models provide forecasts launched at 00Z and 12Z. From those forecasts, the first 6 h of atmospheric forecasts are rejected to allow for the spinup of the atmospheric fields, mostly related to the formation of clouds, affecting the precipitation and surface radiation variables. Hence, we use the hours 06 to 17 of each forecast to force CIOPS-E. To avoid time discontinuities between successive forecasts, we perform a time interpolation between the 12 h-spaced forecasts (00Z and 12Z). For example, the hours 18–24 of the 00Z forecast would be blended to the hours 6–12 of the 12Z forecast as their validity date are the same. The linear interpolation is performed over the first 6 h of the most recent forecast, using coefficients that rapidly decrease for the hours 18–24 (1.00, 0.50, 0.35, 0.25, 0.15, 0.05) to rapidly emphasize the most recent forecast, where errors in atmospheric fields are smaller due to the shorter lead time of the forecasting period. A similar method was used and evaluated for storm surge forecasting, showing the absence of shock in the wind and pressure fields by Bernier and Thompson (2015).

2.3 Mesoscale correction method (spectral nudging)

As the CIOPS-E system is used to provide short-term forecasts of the ocean conditions for applications in environmental emergency response and navigational safety, there is a clear benefit to constrain the mesoscale features, such as Gulf Stream eddies, toward the observed state of the ocean. Moreover, an accurate representation of offshore mesoscale features can affect cross-slope exchanges and water mass properties on the shelf (Brickman et al. 2018). In this context, it is important to constrain the CIOPS-E solution towards such observed states. Here, the RIOPS data assimilative solution is used to constrain the three-dimensional temperature and salinity fields in CIOPS-E. This is achieved using a spectral nudging method (Thompson et al. 2006) applied for wavenumbers of mesoscale eddies and lower.
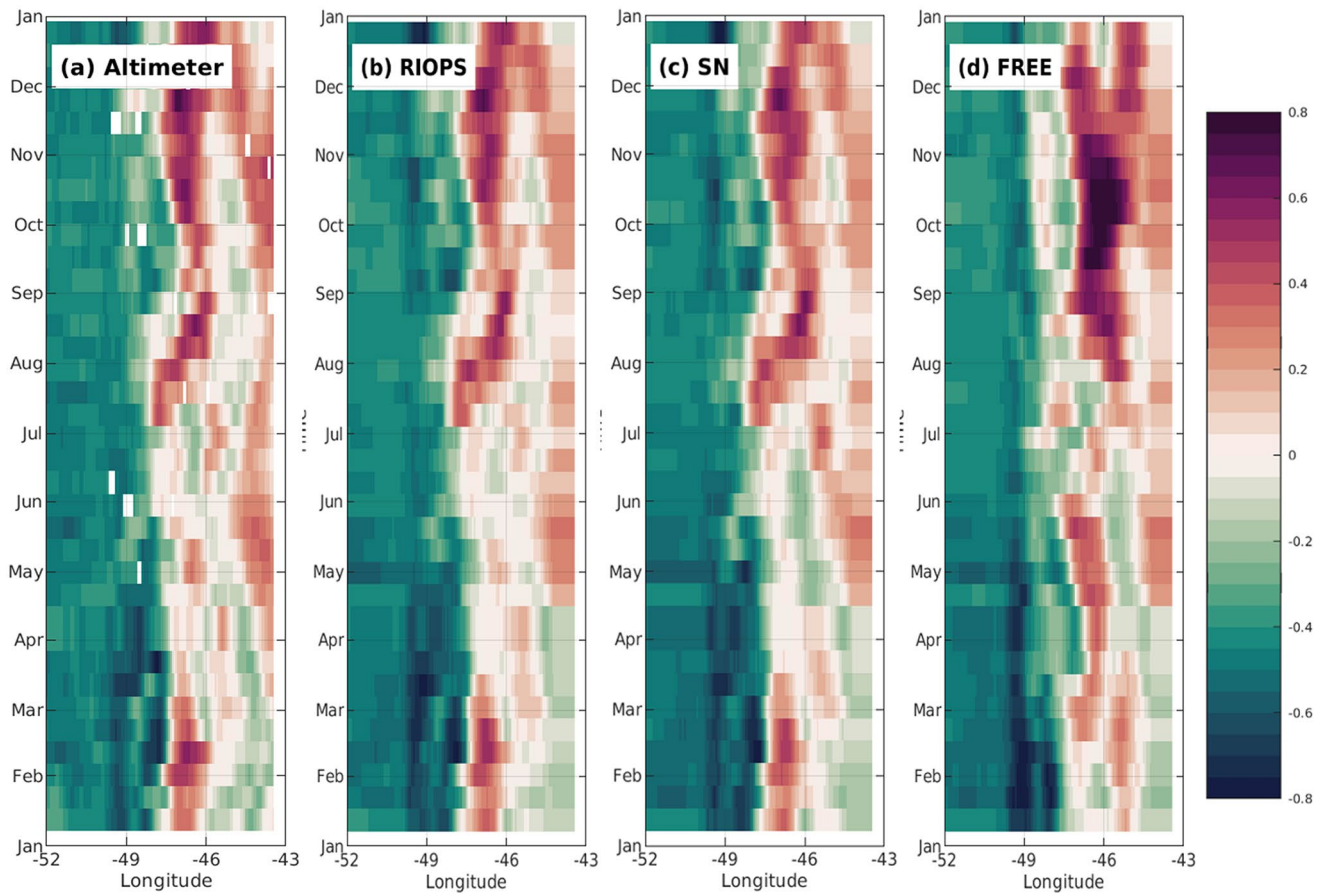
Fig. 2 Sea surface anomaly (m) comparison along Jason 2 altimetry track (see Fig. 1). The four panels show Hovmöller diagrams along the track longitude (ºE) for each altimeter swath at 10-days recur-ring period from January to December 2016 for (**a**) altimeter data (**b**) RIOPS, (**c**) SN-run and (**d**) FREE-run, respectively

These scales are adequately constrained in RIOPS through the assimilation of nadir altimetry in the SAM2 data assimilation scheme, especially over the Gulf Stream regions (Smith et al. 2021; Smith and Fortin 2022). For higher wavenumber bands, the CIOPS-E solution is free to evolve and to generate finer-scale features. Spatially, the spectral nudging is applied over the entire water column but only for regions offshore of the 1500 m isobath (see Fig. 1). On the shelf, satellite nadir altimetry provides a less effective constraint on mesoscale variability due to a variety of factors such as limited spatial coverage and larger errors due to coastal effects (Vignudelli et al. 2019). Recent efforts to develop coastal altimetry products (including the use of wide swath altimetry) may improve this situation, however these data are currently not available over this region. As a result, the approach used here is designed for CIOPS-E to benefit both from the spectral nudging off the shelf and from the improved representation of bathymetry and coastlines on the shelf.

To demonstrate the effectiveness of the spectral nudging method in constraining the CIOPS-E mesoscale circulation off the shelf, we evaluate the SSH anomaly from satellite altimetry with the RIOPS fields and with two distinct CIOPS-E experiments carried from November 2015 to December 2016. The first of the two CIOPS-E experiments, hereafter SN-run, uses the spectral nudging method (as described above), whilst the second experiment is a "free run" without spectral nudging, hereafter referred to as FREE-run. In FREE-run, the mesoscale circulation is not constrained towards the observations and is therefore subject to the effects of the model's internal (chaotic) variability. Two aspects of our implementation of the spectral nudging are evaluated in this section. First, we evaluate the efficiency of the spectral nudging to constrain the mesoscale circulation towards RIOPS off the shelf (and hence indirectly with the observations). Second, we illustrate the capacity in CIOPS-E to develop realistic fine-scale structures over the unconstrained shelf area, but also over the deep-ocean area where the nudging is applied.

Figure 2 compares (a) the SSH anomalies over the period from January to December 2016 along a Jason 2 altimeter track, (b) RIOPS, (c) CIOPS SN-run and

(d) FREE-run. SSH anomaly observations are from the Level-3 near real-time along-track satellite altimetry product for Jason 2, as provided by the Copernicus Marine Service. The Jason 2 track extends from the Avalon Peninsula in Newfoundland, over the Grand Banks of Newfoundland before crossing the energetic eddy region of the Gulf Stream. The altimeter track has a 10-day return period and provides filtered SSH measurements every 14 km along the altimeter track. The satellite altimetry and RIOPS show a strong correspondence of SSH anomalies, both in terms of their amplitudes and variability. This close correspondence reflects the accuracy of the RIOPS data assimilation scheme in constraining the location and amplitude of the mesoscale eddies (Smith and Fortin 2022). The SN-run in turn reproduces quite closely the variability and timing of eddies detected in

the satellite altimetry and in RIOPS, thereby demonstrating the effectiveness of nudging the 3D temperature and salinity fields to constrain the mesoscale features toward the observations. On the other hand, the FREE-run does not reproduce the timing nor the amplitude of the anomalies. This is to be expected as the FREE-run is not constrained in the domain interior and therefore differences accumulate due to the internal (chaotic) variability in the evolution and trajectories of Gulf Stream eddies and other mesoscale features.

In order to show the general impact of the spectral nudging method on the SSH, Fig. 3 presents an example comparing the same experiments for a given date, September 1st 2016, with the daily Copernicus Marine Service Global Ocean Gridded Level-4 Sea Surface Height
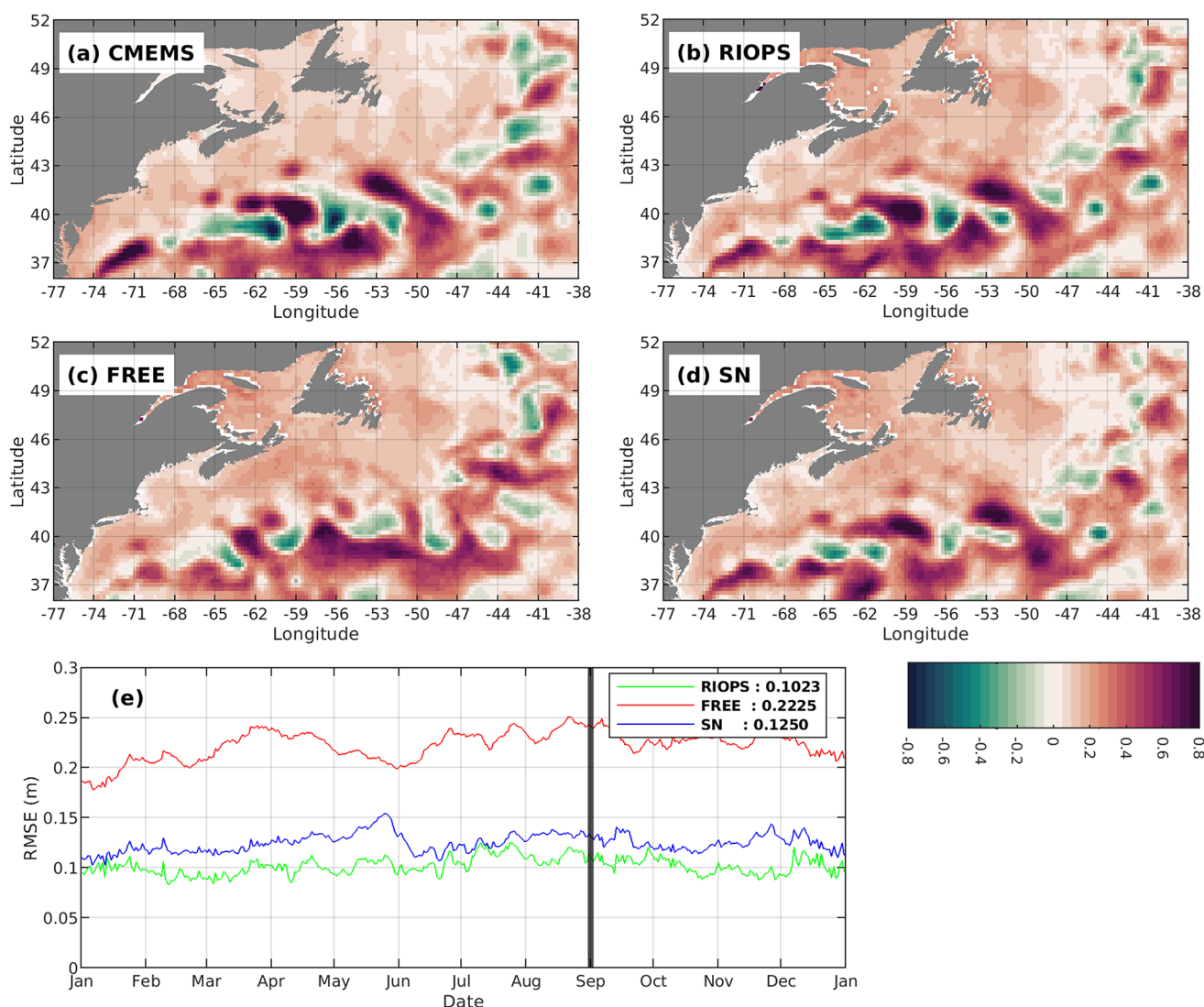
Fig. 3 Comparison of sea level anomaly (m) on September 1st 2016 for (a) CMEMS 1/4° gridded altimetry, (b) RIOPS, (c) FREE-run and (d) SN-run. (e) Time series of the domain-averaged RMSE (m) for RIOPS (green), the FREE-run (red) and SN-run (blue). Averaged RMSE values for the 1-year simulation are shown in the insert

product[1], available on a regular ¼° latitude-longitude grid. To minimize the errors due to smaller-scale circulation features and stronger gradients in the models compared to the Level-4 product, model outputs are interpolated and smoothed to the altimeter-derived ¼° resolution. Conclusions similar to the single-track analysis are found: (i) RIOPS data assimilation accurately constrains the position of mesoscale features, (ii) the SN-run SSH anomaly is well correlated spatially with RIOPS and (iii) larger differences are present for the FREE-run, especially in the position of individual eddies. Note that some small differences are visible in the spatial structures of the SN-run compared to RIOPS in the Gulf Stream. This is expected as the nudging technique tends to gradually decrease differences in the large-scale structures of the 3D temperature and salinity, by applying small corrections at each timestep. This allows for some differences to remain between the two solutions and also allows CIOPS-E to refine the lower-resolution RIOPS solution. The timeseries of the domain-averaged root mean square error (RMSE), presented in Fig. 3, also confirm that the improvement due to the spectral nudging is present over the entire 2016 analysis period, with smaller averaged RMSE for RIOPS (0.102), somewhat larger for the SN-run (0.125), but substantially smaller than in the FREE-run (0.223).

The spectral nudging methodology aims to constrain the mesoscale features towards those in RIOPS, therefore limiting the expression of the model internal variability that would eventually dominate the evolution of the Gulf Stream meanders and eddies. Additionally, the spectral nudging method should allow the higher-resolution 1/36° CIOPS-E to produce finer-scale mesoscale features along the constrained large-scale structure. To explore this, Fig. 4 presents the vorticity fields calculated at 30 m depth for RIOPS and both CIOPS-E experiments. Consistent with previous results, the SN-run shows good correspondence to RIOPS over the area where the nudging is applied. The CIOPS-E simulation shows additional filaments and sharper gradients super-imposed over the mesoscale structures.

Over the shelf and in the GSL, the spectral nudging is not applied in CIOPS-E and mesoscale features are free to evolve. Figure 4 shows more energetic circulations in both CIOPS-E experiments compared to RIOPS, with enhanced mesoscale features over most of the shelf. The water masses in the St. Lawrence Estuary are influenced by the St. Lawrence River plume forming a surface-intensified buoyant coastal current along the south shore of the estuary. This current, referred as the Gaspé Current, can become

baroclinically unstable (Reszka and Swaters 1999) and detach from the coast to partially recirculate cyclonically in the Anticosti Gyre (Sheng 2001; Saucier et al. 2003). The Anticosti gyre is stronger in CIOPS-E with an intensified recirculation due to a stronger Gaspé Current. Both CIOPS-E experiments have eddies in the estuary resulting from baroclinic instabilities in the Gaspé Current, absent from the RIOPS solution. The eddies detaching at the eastern tip of the Gaspé Peninsula, travelling to the southeast in the GSL towards Cabot Strait, are also more energetic in the CIOPS-E experiments. Figure 4 also suggests a stronger and narrower Nova Scotia current closer to shore in CIOPS-E, and a stronger circulation around the southern tip of Nova Scotia and in the Gulf of Maine.

In summary, the actual implementation of the spectral nudging technique applied on offshore 3D temperature and salinity fields combines the advantages of effectively constraining the position of the large-scale circulation (Gulf Stream eddies and meanders) off the shelf, whilst leaving the shelf areas free to develop realistic but unconstrained fine-scale circulation not present in RIOPS.

3 System evaluation

The CIOPS-E evaluation is performed over a 1-year period from March 1st 2019 to February 29th 2020. The simulation is initialized in November 2015 and runs continuously up to the evaluation period. As the operational atmospheric model HRDPS changed significantly in 2018, impacting the near-surface and radiation fields, we focus our analysis of the CIOPS-E results after the atmospheric model's update.

The CIOPS-E simulation is compared to in situ observations and other CCMEP operational analyses (SST and sea ice), to its parent operational system (RIOPS), and to the previous operational system covering the GSL (RMPS-GSL). This approach follows similar evaluations presented for coastal ocean prediction systems developed for the North-West European Shelf (Maraldi et al. 2013; Tonani et al. 2019) and for the Seas around Japan (Sakamoto et al. 2016, 2019), focusing on variables that are important for the simulation of oil drift. The evaluation presented here aims to assess the CIOPS-E performance with respect to other operational systems and products covering the region of interest. The focus is to evaluate (i) tidal amplitudes and phases, (ii) the subtidal water level variability, (iii) sea surface temperatures, (iv) water mass properties and (v) the seasonal sea ice cover.

---

[1] Copernicus Global Ocean Gridded SSH available at: https://doi.org/10.48670/moi-00149.
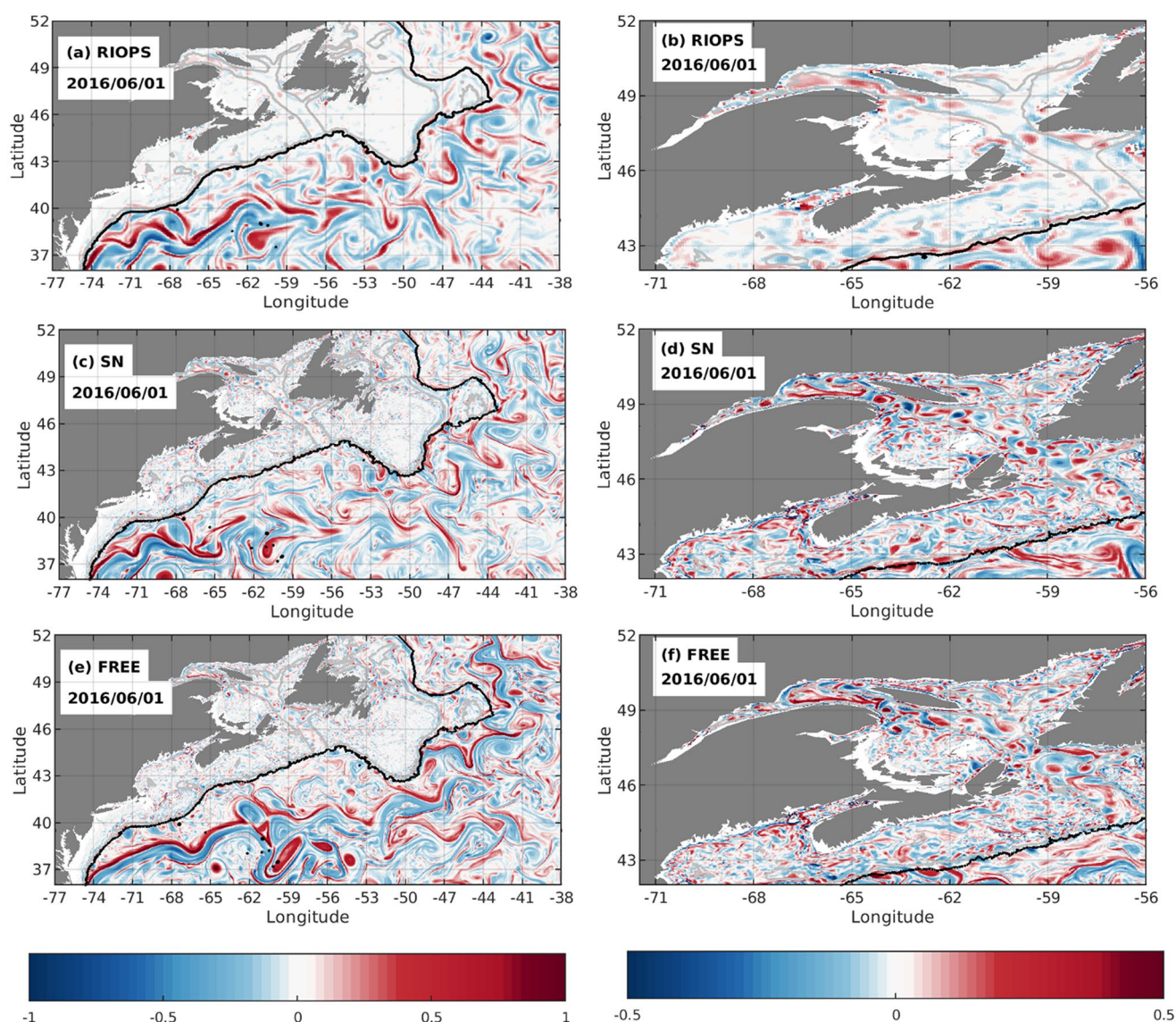
Fig. 4 30 m depth vorticity for June 1st 2016 for RIOPS, the SN-run and FREE-run over the CIOPS-E model domain (**a**, **c** and **e** respectively) and zoomed over the GSL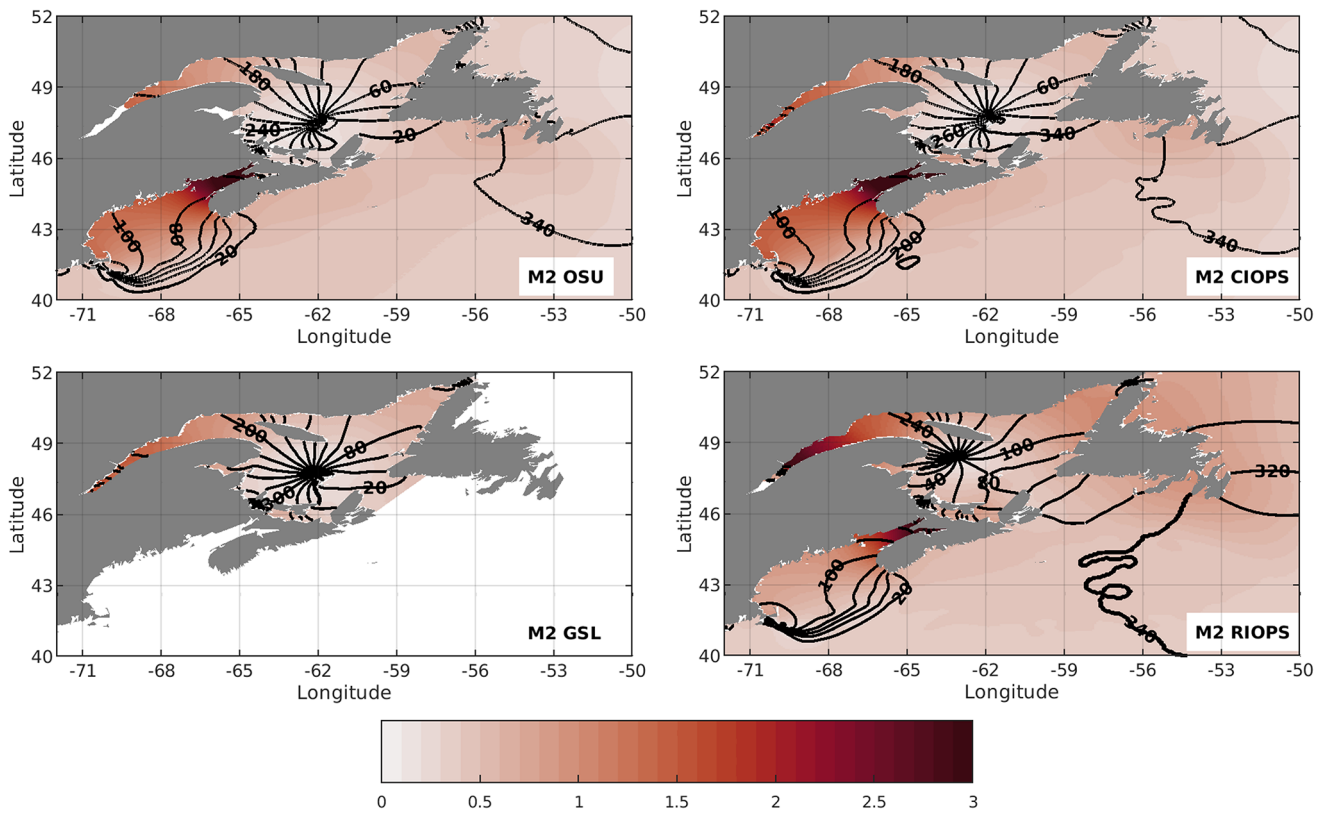 and adjacent shelf waters (**b**, **d** and **f** respectively). Please note the different colour scales between the two columns. The 200 m and 1500 m isobaths are represented by the black and light gray contours respectively

3.1 Tides

As tides over the CIOPS-E domain are amongst the largest in the world, the tidal currents represent the main source of variability in near-surface currents. Therefore, we first evaluate CIOPS-E representation of the main tidal constituents. Tidal amplitudes and phases are computed using the t-tide harmonic analysis package (Pawlowicz et al. 2002) on hourly time series of observed water levels at coastal tide gauges[2] with corresponding simulated sea surface heights.

The simulated timeseries are extracted at the closest model wet point to the tide gauge location. The harmonic analysis is performed over the period from March 1st 2019 to February 29th 2020. We present the results for the principal lunar semi-diurnal tidal constituent (M2) and lunar diurnal constituent (K1) constituents in detail as similar patterns, error structures and improvements are obtained for the other semi-diurnal (N2, S2, K2) and diurnal (O1, P1, Q1) constituents. Additional comparisons for the other main tidal constituents (M2, N2, S2, K1 and O1) at all available coastal tide gauges in CIOPS-E are presented in Paquin et al. (2021a, 2022a).

---

[2] Coastal tide gauge data is available at: https://www.tides.gc.ca/en/tides-currents-and-water-levels for Canadian stations and https://tidesandcurrents.noaa.gov/stations.html for stations in the United States of America.
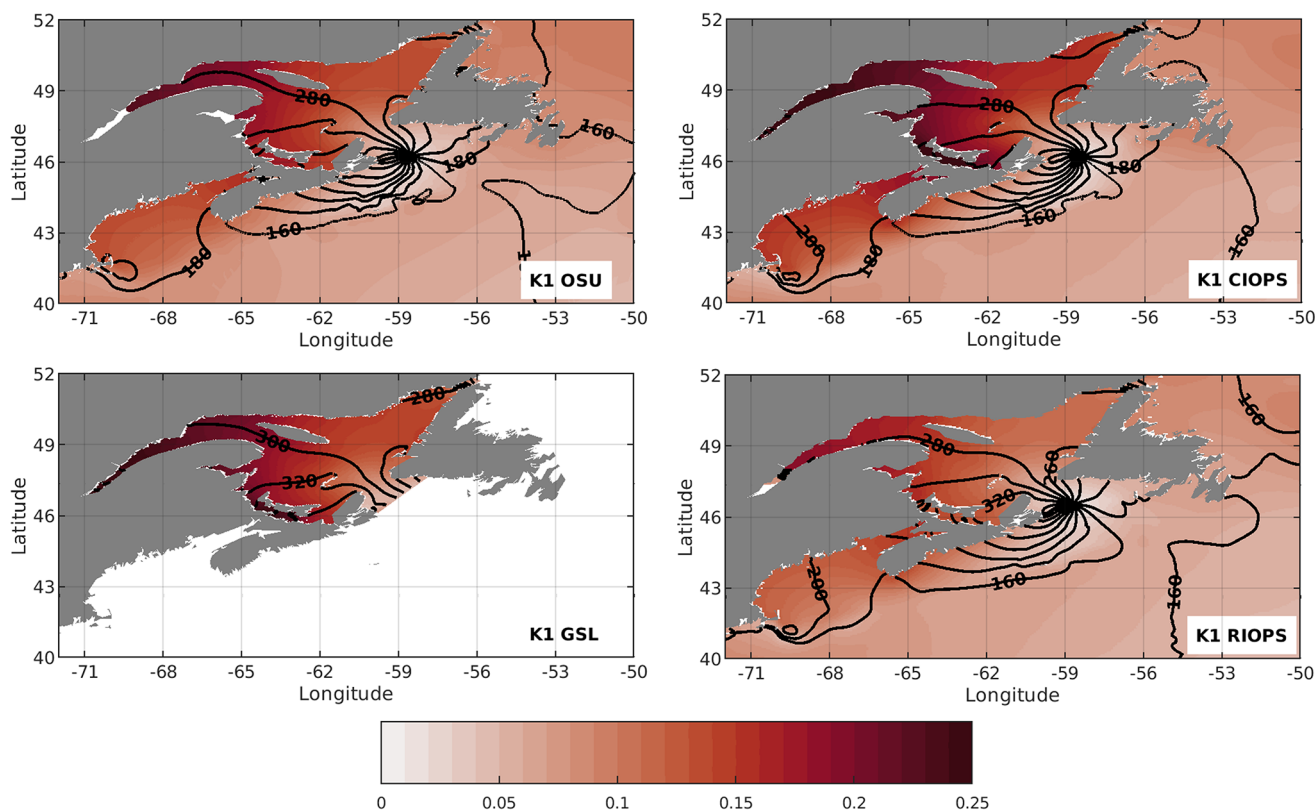
Fig. 5 Co-amplitudes (colours, m) and co-phases (lines, deg) for the principal lunar semidiurnal (M2) tidal constituent: Oregon State University (OSU, top left), CIOPS-E (top right), RMPS-GSL (bottom left) and RIOPS (bottom right)

Figure 5 presents the co-amplitude and co-phase of M2, showing OSU, CIOPS-E, RIOPS and RMPS-GSL. OSU is used as a reference for comparison as it provides the tidal boundary conditions for CIOPS-E. The main M2 features over the region are (i) a resonance in the Bay of Fundy (saturated colours) leading to a tidal range of up to 16 m in the upper bay, (ii) the large amplitudes along the coast of the Gulf of Maine, (iii) an amphidrome located in the central GSL close to the Îles-de-la-Madeleine (station #10 on Fig. 1) and (iv) the increasing amplitude along the St. Lawrence Estuary towards Québec City (#1 on Fig. 1). Comparing CIOPS-E with RIOPS shows a general improvement of the M2 tides in both amplitude and phase (Fig. 5). CIOPS-E reproduces the larger tidal amplitudes and also corrects the phase errors from RIOPS in the Bay of Fundy and in the Gulf of Maine area. The location of the amphidrome in the Central GSL is also closer to the Îles-de-la-Madeleine in CIOPS-E, a significant improvement compared to RIOPS, where the amphidrome is located East of the Gaspé Peninsula. Tidal amplitudes and phases across the GSL are also better represented. CIOPS-E shows a better agreement with OSU for amplitudes in the Northeastern Gulf, while RIOPS shows an overestimation. The increasing amplitudes along the St. Lawrence Estuary is also better represented in CIOPS-E as RIOPS tends to overestimate the signal. Although tidal amplitudes are similar between CIOPS-E and the RMPS-GSL, CIOPS-E significantly improves the M2 phases around the amphidrome. Similar results are obtained for the other semi-diurnal constituents: N2, S2 and K2 (Paquin et al. 2021a, 2022a). CIOPS-E reproduces the resonant system for the semi-diurnal tides in the Gulf of Maine and Bay of Fundy despite an overestimation of the M2 amplitudes. This overestimation reaches a maximum of 30 cm at the St. John Harbour (#19) and Eastport (#20) coastal tide gauges, but still represent an 10% error of the total M2 amplitude (see Fig. 7 presented later).

A similar comparison is presented in Fig. 6 for the K1. K1 over the model domain is characterized by an amphidrome located East of Cape Breton Island (where station #16 is located on Fig. 1), and with increasing amplitudes along the western GSL and in the St. Lawrence Estuary. Generally, K1 amplitudes from CIOPS-E in the GSL are closer to OSU, improved with respect to the underestimated ones from RIOPS. CIOPS-E also reproduces the observed increase in K1 amplitude in the Northumberland Strait (southwestern GSL, see stations #8 and #9), absent from

Fig. 6 Co-amplitudes (colours, m) and co-phases (lines, deg) for the lunar diurnal (K1) tidal constituent: Oregon State University (OSU, top left), CIOPS-E (top right), RMPS-GSL (bottom left) and RIOPS (bottom right)

the RIOPS and OSU reference solutions. CIOPS-E phases, however, are slightly degraded in the GSL, by up to 5° (~20 min), compared to RIOPS.

In general, the improvements of the tides compared to RIOPS and RMPS-GSL are due to multiple factors: (i) the application of tidal boundary conditions closer to the region of interest compared to RIOPS[3] and (ii) a refined resolution of the coastline and addition of higher resolution and more accurate bathymetric data, especially for the GSL and the St. Lawrence Estuary.

At coastal tide gauges, quantitative differences between modelled and observed tides are calculated using the complex differences (Foreman et al. 1995; Soontiens et al. 2016), defined as:

$$D = [(A_O \cos g_O - A_M \cos g_M)^2 + (A_O \sin g_O - A_M \sin g_M)^2]^{1/2} \quad (2)$$

where A_O, A_M, g_O and g_M are the observed and modelled amplitudes and phases, respectively. Figure 7 compares the complex differences calculated at the coastal tide gauges for tidal constituents M2 and K1, showing CIOPS-E, RIOPS, RMPS-GSL and OSU. Stations are organized from the Upper St. Lawrence Estuary, through the GSL, around Newfoundland, the Bay of Fundy – Gulf of Maine, ending southward along the East Coast of the United States (see Fig. 1 for geographic locations and Table 2 for station names).

CIOPS-E improves the representation of the M2 tide with smaller complex differences compared to RIOPS and RMPS-GSL for all but one station. The reduction of the complex differences, compared to RIOPS, is especially important over the GSL and the St. Lawrence Estuary, where the improved representation of the bathymetry and coastline, combined with the adjusted bottom friction, significantly improves the propagation of the tide and the location of the amphidrome. Despite a significant improvement of the complex differences in the Bay of Fundy – Gulf of Maine area compared to RIOPS (stations 18 to 22), large errors are still noted in the CIOPS-E

---

[3] RIOPS's domain covers from 26°N in the North Atlantic to 44°N in the North Pacific (Smith et al. 2021).

Table 2 Statistics for daily-averaged residual water level time series (see Fig. 1 for stations locations)

No	Tide Gauge	RMSE			Correlation			Gamma-squared		
		CIOPS-E	RIOPS	RMPS-GSL	CIOPS-E	RIOPS	RMPS-GSL	CIOPS-E	RIOPS	RMPS-GSL
1	St-François-de-l'Île-d'Orléans	0.097		0.112	0.90		0.87	0.21		0.28
2	St-Joseph-de-la-Rive	0.053	0.132	0.104	0.95	0.71	0.79	0.10	0.62	0.39
3	Rimouski	0.043	0.060	0.093	0.93	0.89	0.57	0.14	0.28	0.67
4	Sept-Îles	0.030	0.045	0.089	0.97	0.94	0.69	0.06	0.14	0.53
5	Rivière-au-Renard	0.048	0.060	0.093	0.88	0.84	0.36	0.26	0.40	0.98
6	Belledune	0.035	0.047	0.091	0.95	0.92	0.64	0.09	0.16	0.59
7	Lower-Escuminac	0.041	0.044	0.094	0.94	0.94	0.64	0.11	0.13	0.59
8	Shediac Bay	0.045	0.061	0.095	0.95	0.91	0.76	0.09	0.17	0.42
9	Charlottetown	0.046	0.061	0.100	0.92	0.86	0.52	0.15	0.27	0.72
10	Cap-aux-Meules	0.040	0.061	0.095	0.92	0.83	0.47	0.15	0.34	0.85
11	Port-aux-Basques	0.036	0.045	0.095	0.93	0.89	0.28	0.13	0.21	0.93
12	St-Lawrence	0.037	0.046		0.95	0.91		0.11	0.17	
13	Argentia	0.040	0.051		0.94	0.90		0.11	0.19	
14	St John	0.039	0.055		0.97	0.93		0.07	0.14	
15	Bonavista	0.035	0.054		0.97	0.93		0.07	0.15	
16	North Sydney	0.031	0.055	0.091	0.96	0.87	0.59	0.08	0.25	0.66
17	Halifax	0.036	0.053		0.95	0.87		0.11	0.24	
18	Yarmouth	0.039	0.049		0.93	0.88		0.15	0.23	
19	St John	0.051	0.069		0.87	0.75		0.25	0.48	
20	Eastport	0.043	0.060		0.91	0.81		0.22	0.44	
21	Bar Harbor	0.031	0.041		0.96	0.93		0.10	0.17	
22	Wells	0.032	0.042		0.97	0.94		0.08	0.13	
23	Boston	0.033	0.037		0.97	0.95		0.08	0.10	
24	Woods Hole	0.029	0.044		0.97	0.93		0.06	0.14	
25	Montauk	0.028	0.043		0.98	0.95		0.05	0.11	
26	Sandy Hook	0.035	0.041		0.98	0.97		0.05	0.07	
27	Atlantic City	0.039	0.050		0.97	0.95		0.06	0.09	
28	Lewes	0.036	0.048		0.98	0.96		0.05	0.08	
29	Duck	0.043	0.052		0.96	0.94		0.07	0.11	

complex differences, due mostly to an overestimation of the M2 amplitudes (also visible on Fig. 5). We suspect that these errors are due to a lack of detail in the representation of the complex coastline and bathymetry, affecting the tidal resonant system. This misrepresentation adds to modifications related to the minimum model water depth, necessary in the absence of a wetting-drying scheme in the current NEMO version. We expect significant improvements adding such scheme in future versions of CIOPS-E.

For K1, complex differences in CIOPS-E are also significantly reduced compared to RIOPS and RMPS-GSL, for most stations. Besides improvements in the upper St.

Lawrence, CIOPS-E also better represents the K1 tide in the Northumberland Strait (between Prince Edward Island and the mainland), namely the Shediac Bay (#8) and Charlottetown (#9) tide gauges. This is due to an improved resolution of the coastline and an updated bathymetry in the 1/36° grid. One might note that CIOPS-E has an improved skill compared to OSU for both stations, where large differences were noted on Fig. 5. While amplitudes are similar between CIOPS-E and RMPS-GSL (Fig. 5), improvements in the K1 phase explain the general reduction of the complex differences in CIOPS-E.
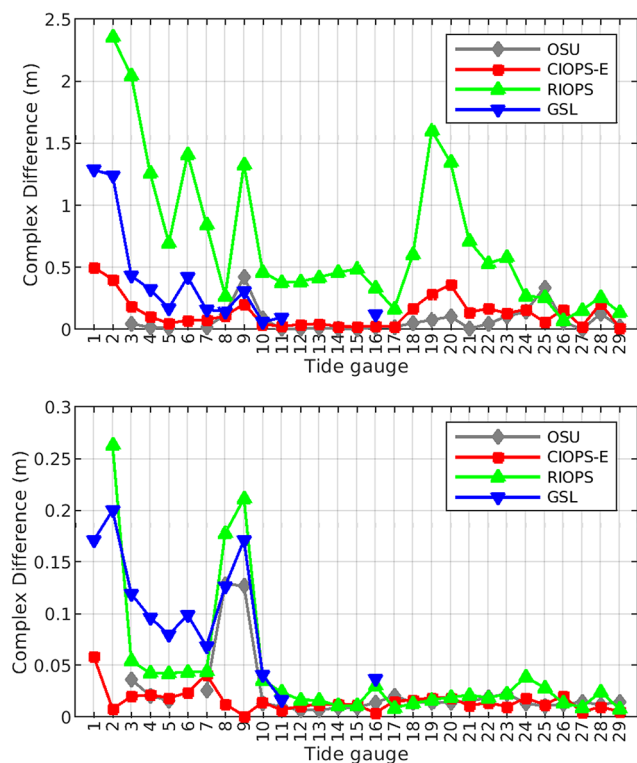
Fig. 7 Complex differences (m) calculated at coastal tide gauges for tidal constituent M2 (top) and K1 (bottom) for CIOPS-E (red squares), RIOPS (green triangles), RMPS-GSL (blue reversed triangles) and OSU (grey diamonds). Stations are numbered according to Fig. 1 (and Table 2) and organized from the St. Lawrence Estuary towards the GSL, Newfoundland, Bay of Fundy – Gulf of Maine, ending with the East Coast of the United States

3.2 Sub-tidal water levels

In this section we compare the modelled residual water level from CIOPS-E, RIOPS and RMPS-GSL over the 1-year analysis period, and its variability compared to observations at the selected coastal tide gauges (see Fig. 1). The representation of residual water levels and their impact on
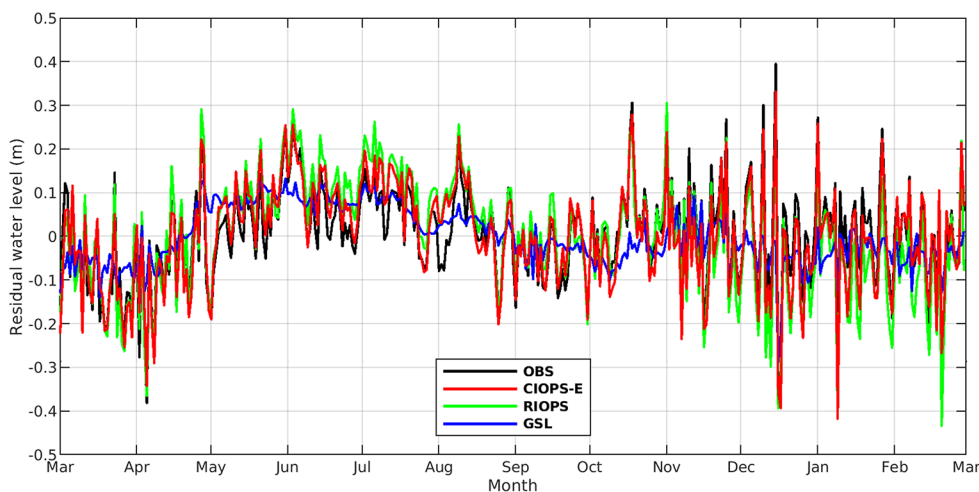
circulation during extreme events is important to navigation safety and emergency response, as the potential for accidents is greater. Residual water levels are calculated by removing the tidal reconstruction using the t-tide harmonic analysis coefficients. The mean water levels at each station are removed respectively from observations and models.

Figure 8 shows the daily averaged residual water levels at the Rimouski tide gauge. RIOPS and CIOPS-E reproduce well both the high-frequency synoptic response to passing weather systems and the seasonal variability. They also both reproduce well the increased variability in winter associated with stronger storms and atmospheric systems, compared to summer. The RMPS-GSL does not capture the high-frequency residual water level variations. In its boundary conditions, the RMPS-GSL only includes tides and climatological temperature and salinity profiles and, therefore, no storm surge signal enters the domain from the North Atlantic. Moreover, the inverse barometer effect on the model's sea surface is not included in the RMPS-GSL, resulting in the large underestimation of the locally-generated residual water level variability.

Figure 9 presents a domain-wide evaluation of the daily averaged residual water levels for the different systems, using the root-mean-squared errors (RMSE) and the gamma-squared score. The gamma-squared score (Thompson et al. 2003; Bernier and Thompson 2010) is defined as the variance of the difference between the observation and the modelled prediction, divided by the variance of observations. A perfect model would have a score of zero and a score of 1 indicates that the system is no better than using a constant value (or persistence).

Geographically, both CIOPS-E and RIOPS present smaller RMSE and gamma-squared scores over the East Coast of the United States (#21–28). Errors then increase in the Bay of Fundy area (#18–20) and reach their maximum values in the GSL and Estuary (#1–11). Table 2 presents the RMSE, correlation and gamma-square scores for each coastal tide gauge. Generally, CIOPS-E shows smaller errors compared to both RIOPS and RMPS-GSL. Improvements

Fig. 8 Daily-averaged residual water levels (m) at the Rimouski coastal tide gauge (station #3 on Fig. 1) from March 1st 2019 to February 29th 2020: Observations (black), CIOPS-E (red), RIOPS (green) and RMPS-GSL (blue)
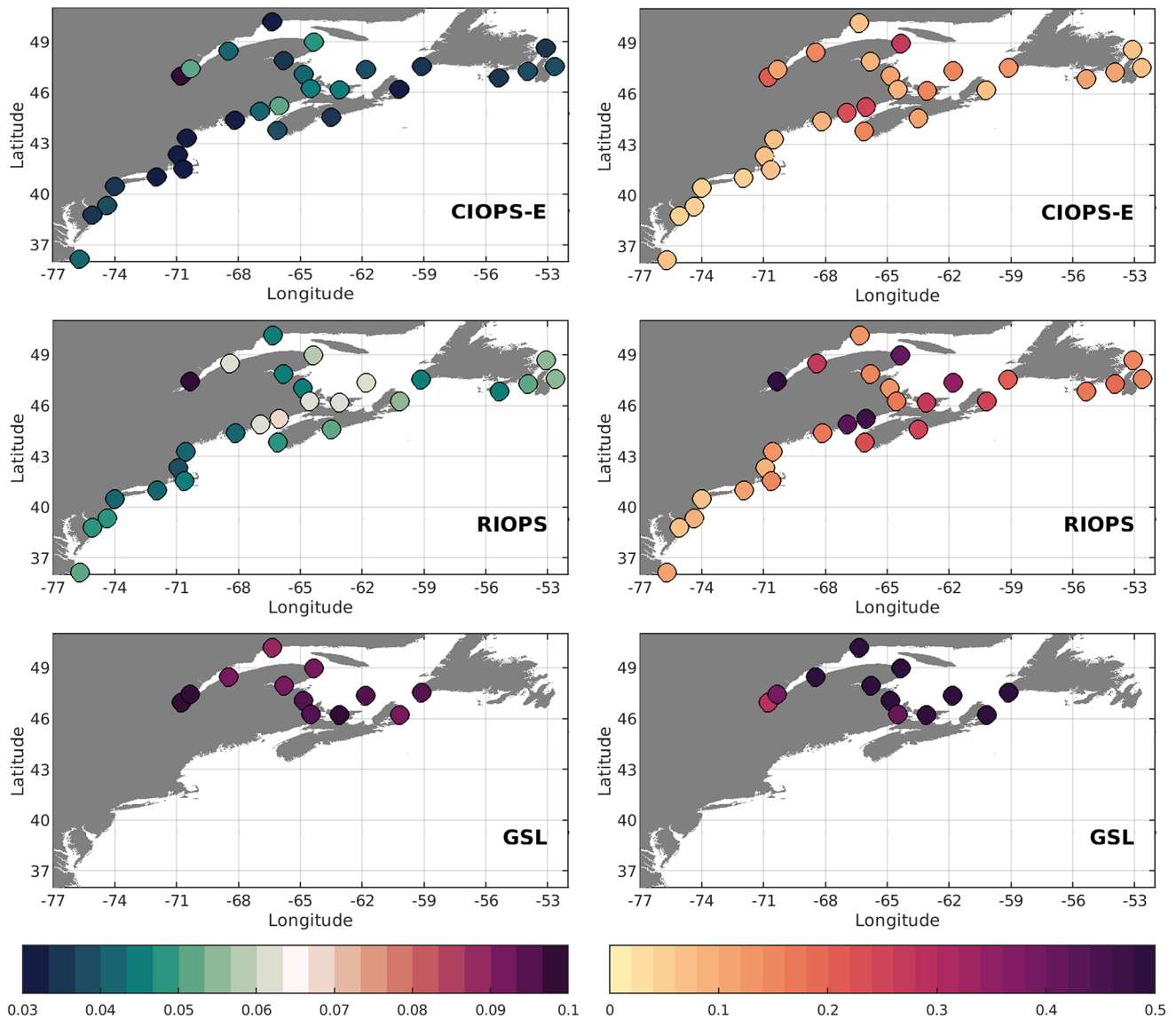
Fig. 9 Root-mean-square errors (m; left) and gamma-square score (right) for daily averaged sub-tidal water levels at coastal tide gauges for CIOPS-E (top), RIOPS (center) and RMPS-GSL (bottom). Detailed values are presented in Table 1

are clearly visible for the Bay of Fundy, where RIOPS is limited due to its coarser resolution. Similar conclusions are shown for the Northumberland Strait, with improvements at the Shediac Bay (#8) and Charlottetown (#9) stations. Significant improvements are also visible in the GSL, where CIOPS-E, show better results for all performance metrics presented in Table 2. As previously mentioned, the RMPS-GSL has the largest errors for all stations across the GSL as it lacks the external forcing that drives much of the residual water level variability. Despite significant improvements in CIOPS-E, both CIOPS-E and RIOPS show similar error structure with larger errors in Cap-aux-Meules, Îles-de-la-Madeleine (#10), increasing at the eastern Gaspé Peninsula station in Rivière-au-Renard (#5) and also at Rimouski (#3). This error is likely linked with errors in the steric structure related to the representation of the Gaspé Current.

Similarly, CIOPS-E and RIOPS have their largest errors at their uppermost station in the St. Lawrence Estuary, namely St-Joseph-de-la-Rive (#2) for RIOPS and Saint-François-de-l'Île-d'Orléans (#1) for CIOPS-E, due to limitations in the resolution of the narrow St. Lawrence Estuary, and the complex dynamics and interactions with the boundary conditions and large freshwater discharge.

3.3 Sea surface temperature

Sea surface temperatures indirectly provide information on near-surface conditions and stratification (an indirect indicator for mixed-layer properties), required to inform oil spill modelling (fate and behaviour) and emergency response in the field such as the use of temperature sensitive chemical dispersants during spills. Here we evaluate the representation of seasonally-averaged SST
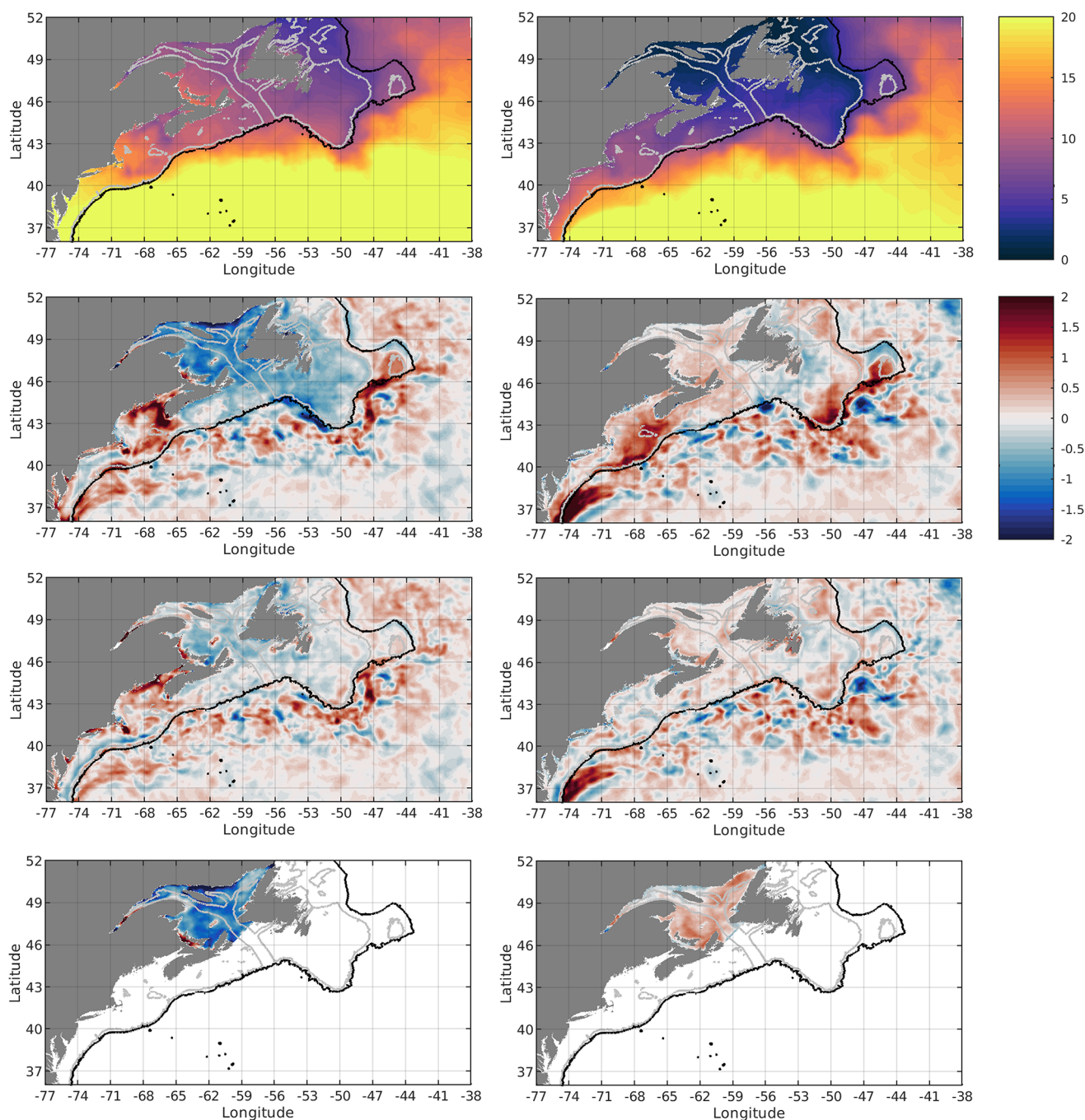
Fig. 10 (1st row) CCMEP SST Analysis (°C) averaged from (left) April to September 2019 and (right) October 2019 to March 2020. Simulation minus CCMEP SST (°C) for CIOPS-E (2nd row), RIOPS (3rd row) and RMPS-GSL (4th row). The 200 and 1500 m isobaths are represented by the grey and black contours, respectively

in the different systems against the daily CCMEP SST analysis product[4] (hereafter CCMEP SST). The CCMEP SST analysis is a daily satellite-derived gridded product on a 0.1° resolution grid using an Optimal Interpolation methodology supplemented with in situ observations from surface buoys (Brasnett 2008; Brasnett

and Surcel-Colan 2016). Note that the CCMEP SST analyses are assimilated in RIOPS. The analyses are also used as surface boundary conditions for the atmospheric forecasts (RMPS-GSL, RDPS and HRDPS) used to force the three different ocean prediction systems evaluated here.

Figure 10 presents the average SST for two periods, (i) spring-summer (April to September) and (ii) fall-winter

---

[4] CCMEP SST analyses data available at: https://podaac.jpl.nasa.gov/dataset/CMC0.1deg-CMC-L4-GLOB-v3.0.

Table 3 Near-surface (0–20 m) regional mean biases and RMSE for temperature (salinity) over the Gulf of St. Lawrence (GSL), Grand banks of Newfoundland and Labrador Shelf (GBN-LS), Gulf of Maine and Scotian Shelf (GoM-ScS), and all profiles located at depth greater than 1500 m (Deep). Statistics for salinity are presented between parentheses. Number of observations represent the total number of profiles valid at the surface for each region. The system with the smallest error is shown in bold

Region	# obs	Mean Bias			RMSE		
		CIOPS-E	RIOPS	RMPS-GSL	CIOPS-E	RIOPS	RMPS-GSL
GSL	1227 (1226)	**-0.06 (0.23)**	0.51 (-0.41)	0.34 (-0.34)	**1.60 (1.44)**	1.85 (2.13)	1.94 (1.64)
GBN-LS	1411 (1276)	**0.03** (0.10)	0.30 **(0.04)**		1.3 (0.39)	**1.26 (0.40)**	
GoM-ScS	979 (908)	0.51 **(0.24)**	**0.09** (-0.47)		1.69 (0.56)	**1.58 (0.84)**	
Deep	2766 (2134)	0.20 (0.07)	**0.09 (0.05)**		1.89 **(1.65)**	**1.75** (1.66)	

(October to March). The first period allows to evaluate the development of the summer surface stratification after the sea ice melt period and through the summer. The second period, from October to March, allows to identify potential delays in the wintertime heat extraction from the ocean to the atmosphere.

Offshore, the SST differences are very similar between RIOPS and CIOPS-E, showing the accuracy of the spectral nudging method applied in CIOPS-E to constrain the SST towards RIOPS's solution. Differences between the two systems are larger near the shelf break, where the spectral nudging is relaxed to reach zero on the shelf.

On the shelf, differences are generally larger in CIOPS-E as RIOPS assimilates SST. The larger differences are expected as RIOPS assimilates precisely the CCMEP SST analysis used in this comparison, and significant increments are used in RIOPS to maintain the SST quite close to the CCMEP SST analyses. Indeed, this was done intentionally with overly small observation errors to reduce initialization shock for coupled modeling (Smith et al. 2018 for details). Some small-scales features are more clearly defined in the models compared to the CCMEP SST analysis, despite the assimilation of satellite and in situ observations in the latter. Such features include the representation of the inshore and offshore branches of the Labrador Current, visible in both RIOPS and CIOPS-E as colder differences, especially in fall-winter. CIOPS-E also simulates a stronger and colder current along the northern section of Orphan Basin (OB on Fig. 1), a feature absent from the CCMEP SST and weaker in RIOPS.

All three systems show large-scale cold (warm) errors with respect to the CCMEP SST analysis over much of the GSL during spring-summer (fall-winter). Differences are generally larger for CIOPS-E and RMPS-GSL compared to RIOPS. All systems have warmer waters around the Îles-de-la-Madeleine in spring-summer. This local maximum, related to the shallow waters around the archipelago, is not captured in the CCMEP SST analysis. Similarly, summer-time warming in Northumberland Strait (between Prince Edward Island and New Brunswick) is stronger in all systems compared to CCMEP SST. Compared to an early version of the CIOPS-E system (Paquin et al. 2022a), the

adjustment of the vertical mixing significantly improves SST results in the GSL area, especially in summer, reducing SST biases from 4°C to less than 2°C.

CIOPS-E shows warmer temperatures in spring-summer southwest of Nova Scotia, in the Bay of Fundy and along the coast in the Gulf of Maine, whilst the largest differences in fall-winter are located from the southwestern tip of Nova Scotia extending over Georges Bank. The exact causes of these warm differences are still under investigation. The current working hypotheses being (1) a general underrepresentation of the low-level clouds and fog in the atmospheric forcing over the area, leading to an overestimation of the shortwave radiation at the surface, warming the near-surface waters; (2) CIOPS-E does not adequately represent the upwelling region located at the southwest of the Nova Scotia and the enhanced mixing caused by the tides around Georges Banks (Garrett et al. 1978).

3.4 In situ temperature and salinity

It is important to evaluate water mass properties as the stratification can be important for oil spill modelling and operational response. We perform here a comparison of the different ice-ocean systems against in situ observations over the CIOPS-E domain area. In situ profiles are quality controlled and uniformly formatted[5] (Coyne et al. 2023). Model-data comparison is done by aggregating the high-resolution (1 m) observational profiles for each of the model vertical layers. The data covers the entire 1-year analysis, and statistics are computed over four different regions (See. Figure 1): (i) Gulf of St. Lawrence, (ii) the Grand Banks of Newfoundland (including Orphan Basin) and Labrador Shelf, (iii) Gulf of Maine and Scotian Shelf, (iv) for waters deeper than 1500 m.

As the operational applications of CIOPS-E are based mainly on near-surface ocean conditions, Table 3 focuses on the mean biases and root-mean-square errors over the first 20 m of the water column. In general, CIOPS-E improves the representation of the near-surface layer in the GSL with smaller biases and RMSE compared to both RIOPS and RMPS-GSL. This gain stems from improvements in the

---

[5] In situ data available at: https://doi.org/10.20383/102.0739.

St. Lawrence Estuary associated with a better representation of the vertical mixing due to winds and the dynamics of the Gaspé Current. The shelf regions outside the GSL present similar error statistics for CIOPS-E and RIOPS, the latter showing slightly better results. This is encouraging as CIOPS-E does not benefit from assimilation of SSTs. Statistics over the off-shelf region generally present larger errors for CIOPS-E, despite the spectral nudging.

In the St. Lawrence estuary, at the head of the Laurentian Channel, tides generate mixing between the warm and salty Bottom Atlantic Layer (BAL) and the Cold Intermediate Layer (CIL), also influencing water properties (Saucier et al. 2003, 2009). The CIL, located generally between 50 and 150 m is partially generated locally in the GSL during the winter but also advected from the Labrador Shelf through Belle-Isle Strait and circulating in the GSL (Koutitonsky and Budgen 1991; Saucier et al. 2003; Smith et al. 2006a, b). All these processes affect the water properties recorded at the IML-4 buoy location, near Rimouski (see Fig. 1). The IML-4 buoy is part of the DFO ocean monitoring program, which maintains several important buoys in the St. Lawrence Estuary and GSL areas. Of the available buoys, the IML-4 buoy has the longest records of temperature and salinity profiles, with minimal data gaps between April and November 2019.

Figures 11 and 12 show the evolution of the temperature and salinity profiles, respectively, from April to November 2019. The winter profiles show a surface mixed layer and CIL extending from the surface to about 100 m, lying above the warmer and saltier BAL. The observed profiles show the spring transition from a two-layer system to a three-layer system with the warming and freshening of the near-surface layer.

The difference plots show that both CIOPS-E and RMPS-GSL tend to reproduce the general structure and evolution of the water masses at IML-4. Both show a warm and salty bias around 25 m and over-stratification of the surface layer, most likely from a lack of vertical mixing and flushing of freshwaters. RIOPS presents a much larger warm and fresh bias at the surface.

Below the surface layer, CIOPS-E better represents the formation and persistence of the CIL, with smaller biases from June to November, although some erosion of the CIL does occur over time, visible as a developing bias at depth. This erosion may be due to a stronger tidal mixing at the head of the Laurentian Channel in CIOPS-E, strengthening the estuarine circulation and eroding the CIL with the BAL. The presence of a salty bias in CIOPS-E below 150 m (Fig. 12) and the mixed condition in the upper estuary (not shown) tend to support this hypothesis. The mid-May 100 m warm bias present in all models might be caused by the misrepresentation of an advective event of CIL waters, visible in the observed temperature profiles. One might also note

that the comparisons at a single point location is subject to spatial aliasing, highlighting the challenges of performing a thorough evaluation in a data-sparse environment.

3.5 Sea ice

Sea ice represents a major challenge for safety in search and rescue operations, as well as for oil spills in ice-infested waters. As such, the capacity of CIOPS-E to adequately represent the spatio-temporal variability of sea ice is a key component of its evaluation. The sea ice over the East Coast of Canada is formed seasonally (as opposed to multi-year ice in the Arctic Ocean) and exhibits significant interannual and spatial variability in response to anomalies in atmospheric and oceanic conditions.

To evaluate sea ice in CIOPS-E, we compare sea ice extent and volume estimates from multiple observational estimates and operational model outputs: namely the Regional Ice Prediction System (RIPS; Buehner et al. 2013, 2016), the weekly Canadian Ice Service (CIS) ice reanalysis (pers. comm.) and operational outputs from RIOPS and RMPS-GSL.

The CIS weekly analysis is produced by manual analysis of a wide variety of satellite, aircraft and in situ observations (Carrieres et al. 1996). This includes RADARSAT2 synthetic aperture radar (SAR) data to derive ice concentration and ice-type distributions. The ice thickness is estimated based on the ice-type distributions, allowing for an estimate of the sea ice volume. The CIS analysis is provided as geographical areas of similar ice-type represented by geometric polygons. The RIPS ice analyses use a three-dimensional variational (3D-Var) assimilation algorithm. The RIPS ice concentration analyses are a combination of passive microwave observations from the Special Sensor Microwave/Imager (SSM/I) and the Special Sensor Microwave Imager Sounder (SSMIS), data from the Advanced Scatterometer (ASCAT), and the manual CIS analyses. RIPS provides sea ice cover information on a 5 km grid covering the North Atlantic and Arctic regions. The RIPS analysis only produces sea ice concentration estimates, without information about the ice thickness.

An important limitation of the evaluation presented in this section is the inter-dependency of the observational estimates and operational model outputs. RIOPS and RMPS-GSL fields are not independent from the CIS weekly ice charts and RIPS ice concentration analyses. RIOPS is constrained to the RIPS ice concentration analyses every 7 days through data assimilation. The RIPS ice concentration is used to initialize RIOPS, but the thickness information comes from the modelled thickness of the ice present in RIOPS at the end of its previous 7-day integration (restart). The RMPS-GSL uses RADARSAT2 image analyses
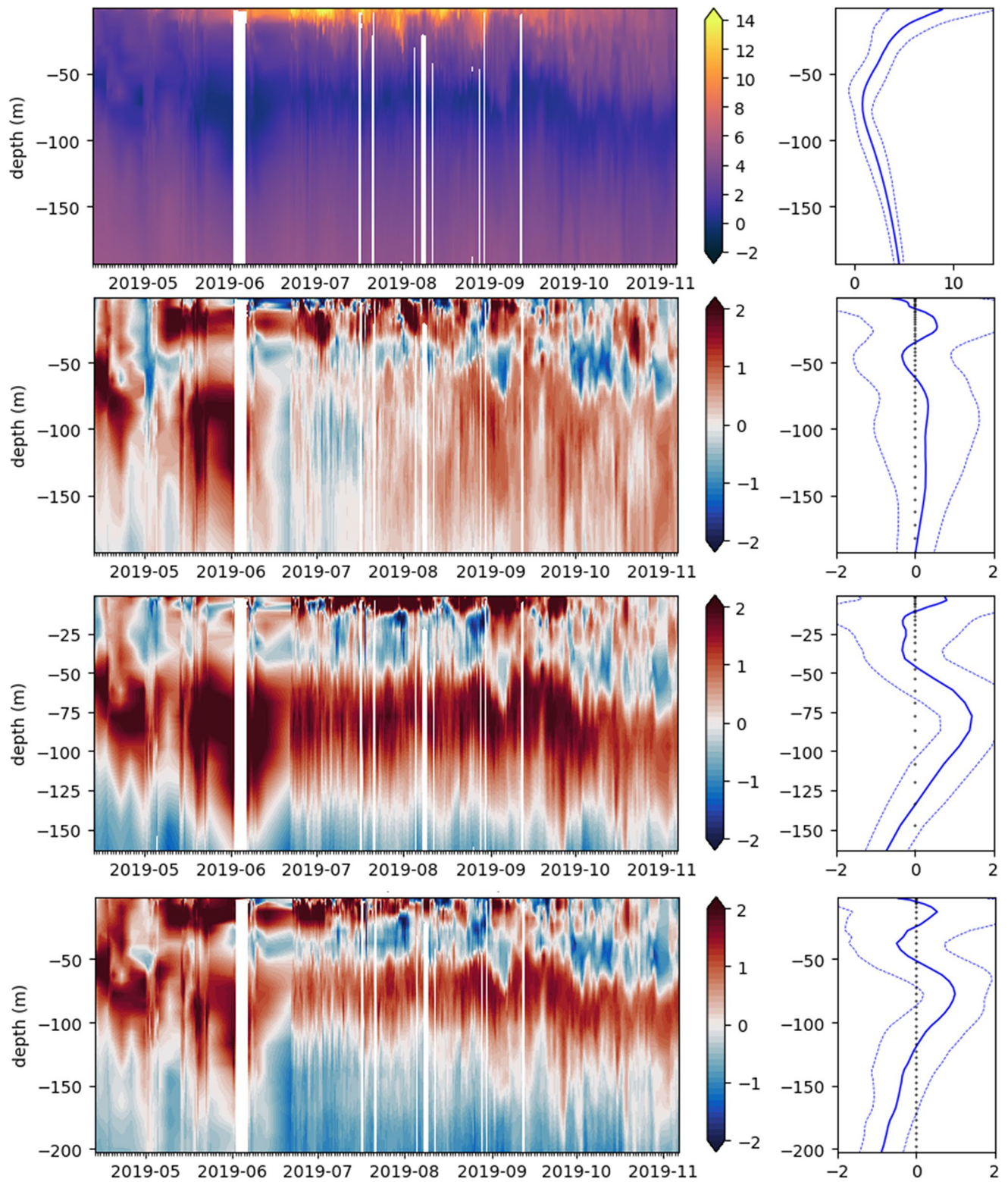
Fig. 11 Evolution of the observed (OBS) temperature profiles (ºC) at IML-4 station (see Fig. 1) in the St. Lawrence Estuary from April to mid-November 2019 (top row). Temperature differences: CIOPS-E minus OBS (2nd row), RIOPS minus OBS (3rd row) and RMPS-GSL minus OBS (bottom row). The left column provides Hovmöller plots and the right column shows the time-averaged profiles (thick lines) plus or minus one standard deviation (dashed lines)
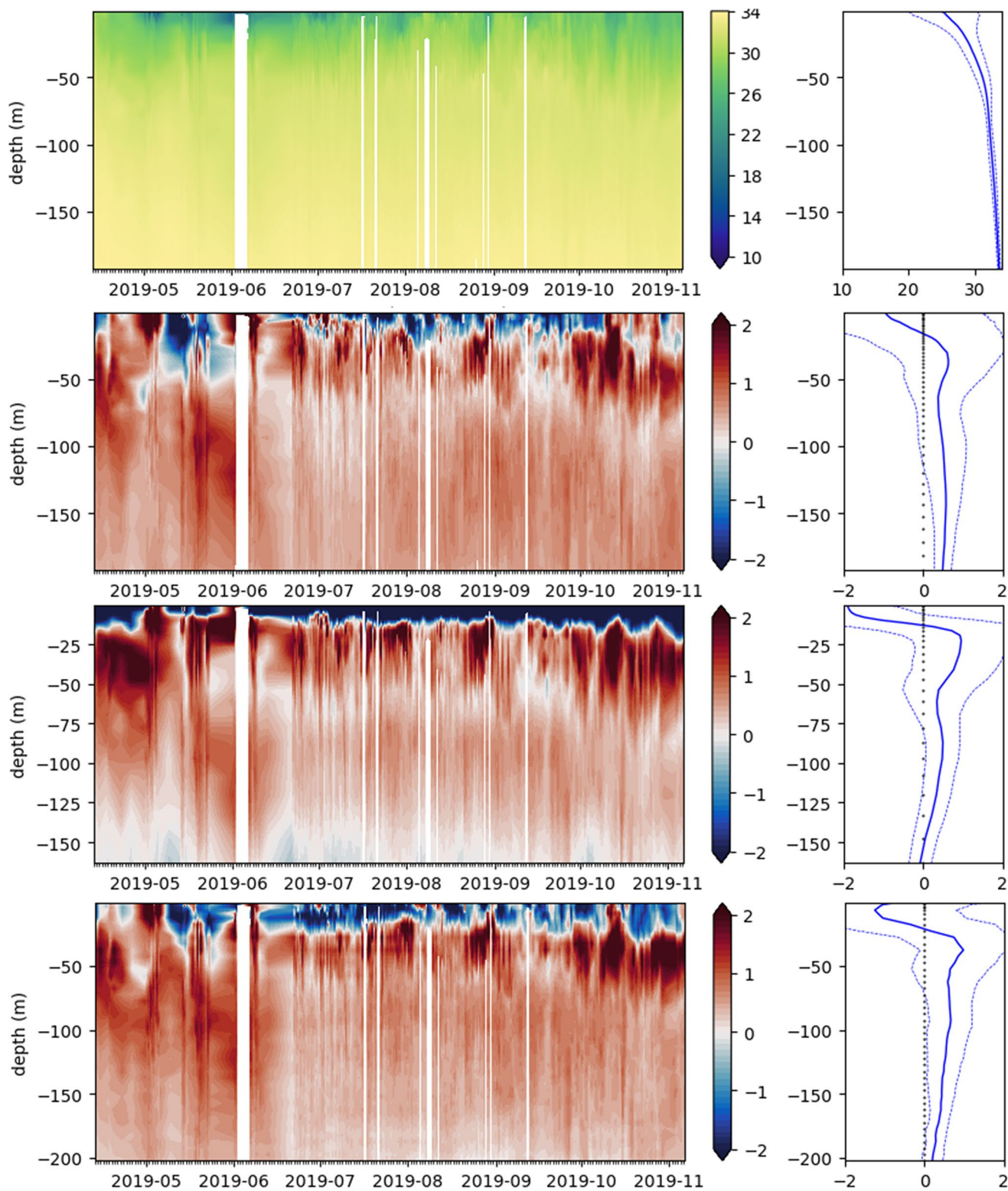
Fig. 12 Same as Fig. 11 but for salinity (PSU)

including both concentration and thickness estimates (stage of development), which are used by CIS analysts in the preparation of the weekly ice charts. Generally, the entire GSL model domain is covered within a three-day period by RADARSAT2 (Pellerin et al. 2004). In this context, similarity between the pairs RIPS/RIOPS and CIS/RMPS-GSL is to be expected. In contrast, the CIOPS-E unconstrained ice simulation should show larger deviations from these observational estimates. The comparison is nonetheless useful, as sea ice is an important integrator of errors and can thus be used to assess imbalances in fluxes across the air-sea interface.

We begin by evaluating the seasonal evolution of sea ice extent and volume over the GSL, here defined as the area enclosed by the Cabot and Belle Isle Straits (Fig. 1). Figure 13 shows the evolution of the sea ice extent and volume over two winters, from November 2018 to March 2020 to capture two complete ice seasons. A threshold of 10% is applied for detection of sea ice concentration in all calculations of sea ice extent and total volume. Sea ice in the GSL starts forming in December and grows to reach a maximum in March before melting completely in May. All data sources agree well on the seasonal cycle and the magnitude

and timing of the maximum sea ice extent and volume. All prediction systems also reproduce well the interannual differences, with more ice present for the winter of 2019 compared to 2020. For each season, the sea ice extent is generally higher in CIS and RIPS observational estimates. RIOPS shows good correlation with RIPS as expected from the initialization procedure explained earlier. The CIOPS-E sea ice extent, despite being freely evolving, follows observational-based estimates reasonably well for both ice seasons, with smaller differences compared to RMPS-GSL. The onset of ice formation is well captured by CIOPS-E but the onset of melt seasons is delayed, with ice remaining present over a longer period in spring compared to all other datasets. This delayed and lengthened melt season are systematically present in CIOPS-E for all winters from 2016 to 2020 (not shown).

To provide an indirect evaluation of sea ice volume, we compare the systems with CIS estimates based on ice-types from the manual analysis of SAR images. As for the sea ice extent, the interannual variability of the ice volume is well capture by all systems, with more ice in the 2019 season compared to 2020. As expected, the RMPS-GSL ice volume is quite similar to the CIS estimates due to their use
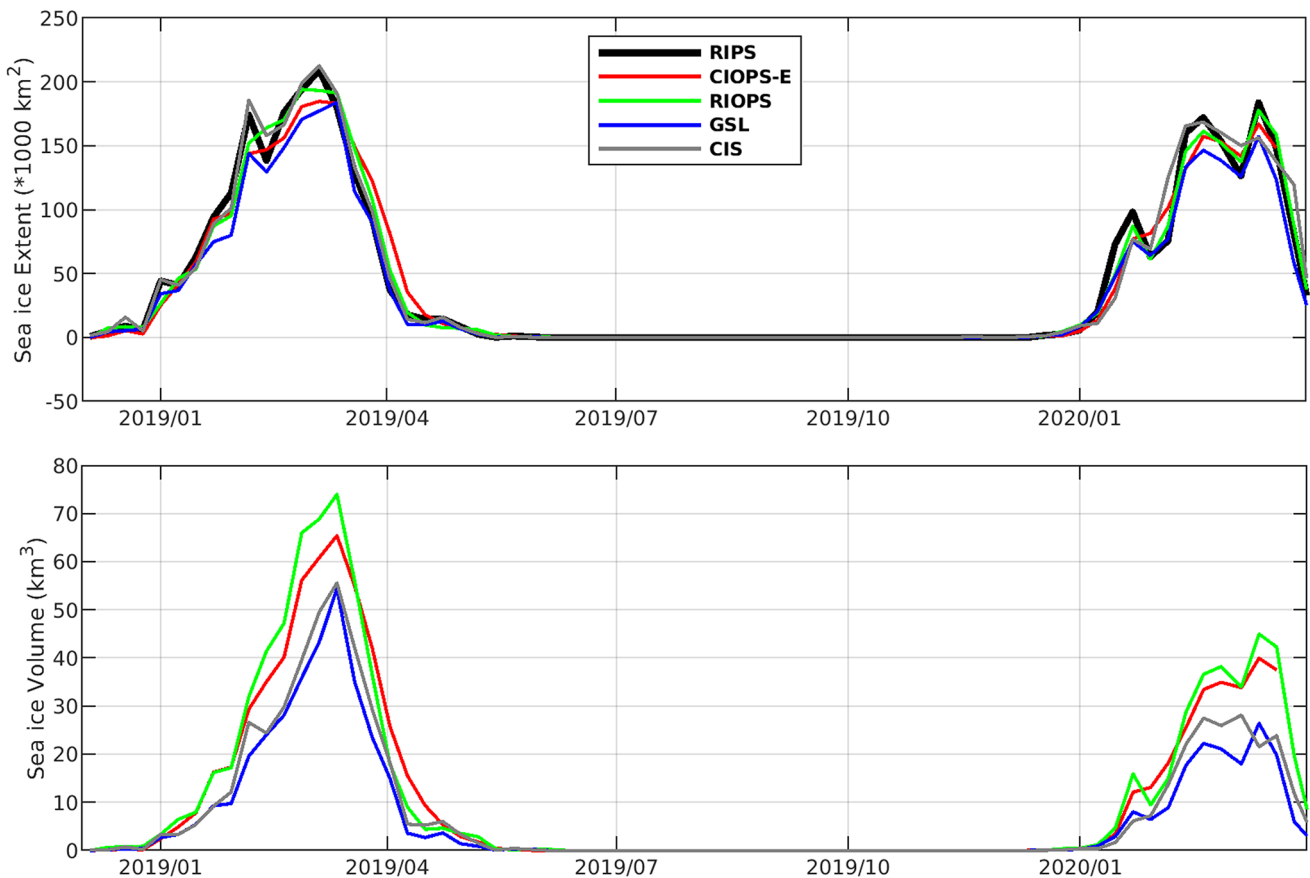
Fig. 13 Sea ice extent (km^2; top) and volume (km^3; bottom) over the Gulf of St. Lawrence from November 2018 to March 2020 from RIPS (black), CIS (grey), CIOPS-E (red), RIOPS (green) and RMPS-GSL (blue)

in the analysis procedure. Both RIOPS and CIOPS-E produce larger ice volumes than CIS due to the simulation of ice dynamics, generating narrow areas of thick deformed ice in convergence areas, as presented below in the spatial analysis.

Next we examine the simulated spatial differences in sea ice over the entire CIOPS-E domain. Figure 14 shows the ice concentration and thickness from RIPS, CIS, CIOPS-E, RIOPS and RMPS-GSL on March 5, 2019, the date of the maximum ice extent calculated from weekly CIS analyses. Observational estimates and model outputs are interpolated to the CIOPS-E grid for comparison, therefore allowing comparison of the fine-scale structure in CIOPS-E. The polygon-based approach used in the CIS manual analyses is clearly visible, resulting in discontinuous regions of uniform sea ice concentration. As RIPS assimilates the CIS data, similar patterns are also visible but with slightly more realistic gradients between polygons. Both observational estimates show the GSL almost entirely covered, with ice concentration above 90%, except for small areas in CIS near Anticosti Island, in the upper St. Lawrence Estuary and along the northern coastline. The ice cover extends south of Cabot Strait, covering the Eastern shore of Cape Breton Island with ice cover rapidly decreasing westward along the Nova Scotia coast. On the Labrador Shelf, ice flowing southward from higher latitudes enters the region and covers a significant fraction of the shelf width.

CIOPS-E sea ice concentration generally presents large-scale structures similar to RIOPS. As CIOPS-E uses a higher horizontal resolution, the ice tends to present finer-scale deformation features such as narrow leads and zones of deformed ice, especially for convergence zones on the western coasts of the Îles-de-la-Madeleine and Cape Breton Island, where the dominant winds in winter would tend to create convergence in sea ice motion, resulting in thickening through ice deformation. The sea ice concentration over the GSL is generally well reproduced in CIOPS-E. The largest difference is the ice-free region in CIOPS-E over the upper St. Lawrence estuary whereas RIOPS and RMPS-GSL have the area covered with around 30% ice concentration. The area of relatively lower concentration on the south shore of Anticosti Island is present in all systems but with different amplitudes and patterns. RIOPS produces the smallest low concentration area, confined to the vicinity of the coast, whilst CIOPS-E generates a narrow opening following the meanders of the eddying circulation. RMPS-GSL generates open water near the Anticosti shore and a much broader area of low concentration values.

Outside the GSL, CIOPS-E reproduces with reasonable accuracy the ice extent south of Cabot Strait and along the Nova Scotia coast, again generating smaller-scale features and filaments compared to RIOPS. The presence of fine-scale structures in CIOPS-E represents a challenge in the evaluation of the simulated ice fields, as these are unresolved in the coarse observational estimates. To avoid penalizing the model due to its higher resolution, the quantitative evaluation of the modelled sea ice fields and their error statistics should eventually be refined to take into account these unrepresented scales in the current observational estimates.

The largest discrepancies in CIOPS-E sea ice concentration and thickness are visible over the Labrador Shelf. Both variables are underestimated near the model northern boundary. This is caused by the absence of a sea ice boundary condition in the current version of CIOPS-E. The southward advection of thicker ice from higher latitudes is therefore neglected and CIOPS-E only generates ice locally. The ice over this area being thinner and more mobile, CIOPS-E underestimates the total sea ice extent and volume as well as the duration of the ice season. The absence of an ice inflow boundary condition in the CICE model is acknowledged as a major limitation of the current system and will be improved in a future version.

4 Summary and conclusions

The Coastal Ice-Ocean Prediction System for the East Coast of Canada (CIOPS-E) was developed and implemented at CCMEP to respond to the growing demand for high-resolution numerical modelling support for coastal aquatic emergency response, hazards in ice-infested waters and in support of other Government of Canada applications (e.g., Search and Rescue and National Defence). CIOPS-E also provides total water levels and currents in support of electronic navigation. CIOPS-E is shown to provide a significant added-value for these applications with respect to both the basin-scale RIOPS system (from which CIOPS-E is downscaled) and the pre-existing coastal system RMPS-GSL.

The CIOPS-E domain covers most of the East Coast of Canada, from the Gulf of Maine to the southern Labrador Shelf, and includes the Gulf of St. Lawrence. The spectral nudging method applied offshore of the shelf break is shown to accurately constrain the temperature and salinity fields towards the data assimilative solution from RIOPS. This allows the reproduction of the observed mesoscale sea level fields (a proxy for mesoscale circulation), otherwise impossible considering the error growth from the model's internal (chaotic) variability in this region. The enhanced resolution in CIOPS-E allows finer-scale variations to evolve according to model dynamics, however, this only leads to a more statistically but not deterministically realistic representation. This poses a difficulty for some applications of CIOPS-E as the positions of small individual eddies would not be
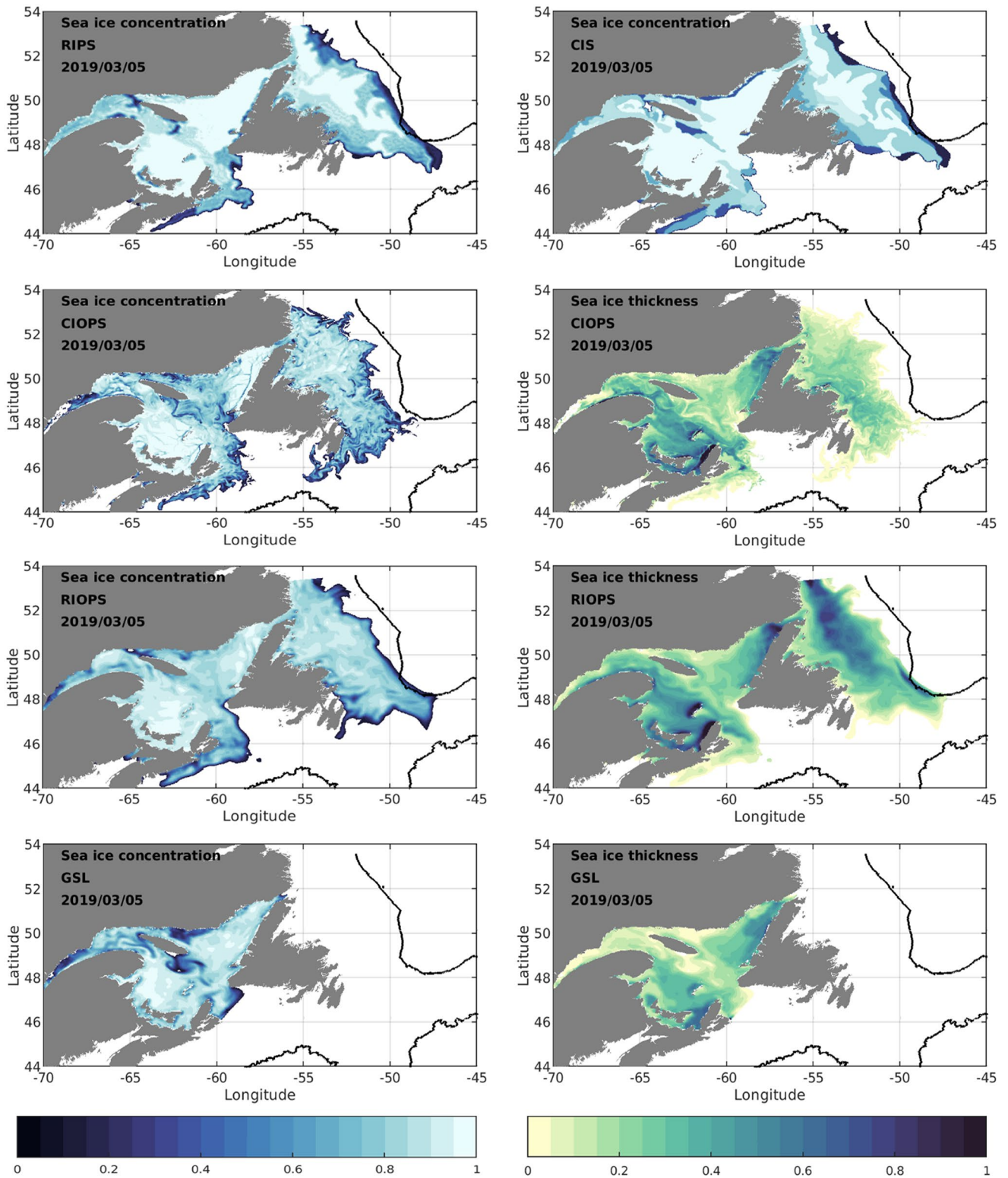
Fig. 14 Sea ice cover (fraction [0 1]) from RIPS (top left) and CIS (top right) for March 5th 2019 at the maximum sea ice extent of the 2019–2020 winter season. Modeled sea ice concentration (left column) and thickness (m, right columns) for CIOPS, RIOPS and RMPS-GSL on 2nd, 3rd and 4th rows respectively. A 10% concentration threshold is applied for concentration and thickness for all figures. The 1500 m isobath is represented by the black contour

constrained to correlate with real-world conditions. In the absence of observations with sufficient spatio-temporal resolution to constrain such scales and their assimilation in RIOPS, application of the spectral nudging technique over a broader wavelength band or on the shelf would not accurately constrain these features in the CIOPS-E solution. Moreover, some energetic chaotic variations in coastal waters, e.g., the meandering of the Gaspé Current in the GSL, are not constrained in CIOPS-E (neither in RIOPS). Quantifying the variability of the fine-scale variations in CIOPS-E using an ensemble approach is the subject of ongoing work. Future work will also explore the possibility of using the new high resolution sea surface height data from the Surface Water and Ocean Topography (SWOT) mission.

Tidal and sub-tidal water levels in CIOPS-E are significantly improved compared to both RIOPS and RMPS-GSL. Improvements are especially significant for the semi-diurnal tides in the Bay of Fundy and in the GSL. In the GSL, CIOPS-E improves the location of the amphidrome at the Îles-de-la-Madeleine, therefore improving both amplitudes and phases across the whole region. In the Gulf of Maine – Bay of Fundy, the representation of the resonant system of the semi-diurnal tides is also greatly improved in CIOPS-E compared to RIOPS, despite showing larger amplitude errors compared to stations in the GSL. A future version of the NEMO system including a wetting-and-drying scheme should eventually improve tides in this challenging region.

CIOPS-E shows an overall improvement in the representation of residual (sub-tidal) water levels for most stations compared to RIOPS. This improvement is especially notable for areas where the increased horizontal resolution in CIOPS-E allows for a more accurate representation of the complex coastline and bathymetry, such as in the St. Lawrence Estuary, the Bay of Fundy and Northumberland Strait.

A comparison with the CCMEP SST analysis shows a persistent summertime cold bias over most of the shelf and GSL areas in CIOPS-E (i.e. where no spectral nudging is applied). Consistently with the analysis of in situ temperature and salinity profiles, the cold surface bias appears to be a consequence of excessive vertical mixing near the surface in CIOPS-E. Despite these limitations, CIOPS-E does improve the overall representation of the water masses and the persistence of the CIL at the IML-4 buoy location in the St. Lawrence Estuary, when compared to the RMPS-GSL system.

The sea ice simulation in CIOPS-E is not constrained by observational estimates and therefore provides an assessment of errors from multiple sources, including the ice model formulation and fluxes from the atmosphere and ocean. In the GSL, CIOPS-E reproduces the seasonality of the ice cover relatively well, with an accurate growth season onset, a slightly underestimated sea ice extent maximum,

and a delayed and lengthened melt period. In terms of ice volume, CIOPS-E provides estimates comparable to RIOPS and CIS/RMPS-GSL. The observed ice spatial distribution at the maximum extent is well reproduced by CIOPS-E compared to RIOPS and to observational estimates for the GSL and the ice exiting through Cabot Strait. A greater number of fine-scale features are found in CIOPS-E with narrow leads and more intense ice convergence zones, compared to both RIOPS and RMPS-GSL. The spatial distribution and interannual variability of the sea ice cover is indirectly constrained by the HRDPS atmospheric forcing, as the atmospheric simulation producing the forcing used the SST and sea ice concentration from the CCMEP SST analysis described earlier. Hence, the information on the sea ice distribution influences the simulation of the near-surface atmospheric variables in HRDPS, which in turns influences the simulation of CIOPS-E ocean surface conditions, ice formation and dynamics. The largest errors in CIOPS-E are related to the absence of a northern ice boundary condition, thereby neglecting the southward advection of thicker ice from the Labrador Shelf.

The CIOPS-E pseudo-analysis evaluated here is used to initialize two different forecasting systems, (i) a CIOPS-E 48 h uncoupled ice-ocean forecasting component using high-resolution atmospheric forcing and (ii) a 84 h coupled atmosphere-ice-ocean forecasting component as part of the Water Cycle Prediction System (Durnford et al. 2018; Dupont et al. 2021). An evaluation of the impacts of coupling the ice-ocean systems with an atmospheric model on forecasting skills and extreme events (e.g. cold air outbreaks, strong synoptic low-pressure systems and hurricanes) will be the focus of a future study. Note that the both forecasting systems initialized using the CIOPS-E pseudo-analysis discussed in this paper constrains the sea ice concentration at initialization of the forecast by using a "direct insertion" method (Pellerin et al. 2004) from the RIPS analyses, therefore reducing the ice forecast errors substantially.

In conclusion, the evaluation of CIOPS-E shows significant improvements over RIOPS and RMPS-GSL for multiple key variables. This demonstrates that CIOPS-E provides a source of high-quality and reliable estimates of ocean conditions in the northwest Atlantic Ocean capable of supporting a variety of high-impact operational applications.

This study also highlights the areas of improvement where further efforts could be directed:

- Adding a wetting-drying scheme could reduce the errors noted in tidal amplitudes and phases for areas such as the Bay of Fundy.
- Adding a northern ice boundary condition would allow advection of thick ice into the model domain, increasing

the quality of ice fields over the Labrador shelf and the Grand Banks.

Work is also currently in progress to evaluate the interannual variability of CIOPS-E over a longer period by performing hindcast simulations, covering 1992-present. The hindcast simulations will allow us to expand data-model comparison using observational data collected by different long-term monitoring programs, such as DFO's Atlantic Zone Monitoring Program[6]. Furthermore, the hindcast will allow the evaluation of modelled versus observed trends noted in areas such as the GSL.

Investigation of CIOPS-E circulation anomalies and the sensitivity of the CIL to atmospheric forcing at different resolutions is also currently underway. The implementation of CIOPS-E pseudo-analysis in the coupled framework of the WCPS will also allow in-depth evaluation of the impacts of atmosphere-ocean-sea ice coupling on surface heat and freshwater fluxes. The impact of coupling on the short-term forecasting skills is a separate but important goal to explore for multiple aspects of the environmental predictions.

Finally, ongoing model development is also required to gradually fill-in the gaps in the current ocean-sea ice forecasting system with the objective to develop a more comprehensive model of the coastal environment, in agreement with international research groups and programs such as COSS-TT (Cirano et al. 2021), Coast Predict[7] and the consensus on coastal model development (Fringer et al. 2019). Such improvements of varying level of complexity range from using more realistic ocean colour data, to coupling with a land-hydrology model for river discharge (and eventually river water temperature), to the addition of wave-ocean processes in the model via a forced or coupled approach. Coastal data assimilation should also eventually be added to the forecasting model in order to better constrain CIOPS-E solution over the shelf as the real-time observational network improves.

like to thank Mercator-Océan International, and in particular, Jérôme Chanut. Finally, we want to thank the two anonymous reviewers for their constructive comments and questions.

Data availability Model outputs and ECCC operational products are available upon request. Copernicus Global Ocean Gridded SSH available at: https://doi.org/10.48670/moi-00149. Coastal tide gauge data is available at https://www.tides.gc.ca/en/tides-currents-and-water-levels for Canadian stations and https://tidesandcurrents.noaa.gov/stations.html for stations in the United States of America. CCMEP SST analyses data is available at: https://podaac.jpl.nasa.gov/dataset/CMC0.1deg-CMC-L4-GLOB-v3.0. In situ data is available at: https://doi.org/10.20383/102.0739. DFO data for the IML-4 buoy are available upon request.

Declarations

Competing interests The authors declare that they have no conflict of interest.

---

[6] AZMP website: https://www.dfo-mpo.gc.ca/science/data-donnees/azmp-pmza/index-eng.html.

[7] https://www.coastpredict.org/.

References

Aguiar E, Mourre B, Juza M, Reyes E, Hernandez-Lasheras J, Cutolo E, Mason E, Tintoré J (2020) Multi-platform model assessment in the Western Mediterranean Sea: impact of downscaling on the surface circulation and mesoscale activity. Ocean Dyn 70:273–288. https://doi.org/10.1007/s10236-019-01317-8

Becker JJ, Sandwell DT, Smith WHF, Braud J, Binder B, Depner J, Fabre D, Factor J, Ingalls S, Kim S-H, Ladner R, Marks K, Nelson S, Pharaoh A, Trimmer R (2009), Von Rosenberg J, Wallace G, Weatherall P (Global Bathymetry and Elevation Data at 30 Arc Seconds Resolution: SRTM30_PLUS, Marine Geodesy, 32:4, 355–371

Bernier NB, Thompson KR (2010) Tide and Surge Energy Budgets for Eastern Canadian and Northeast US Waters. Cont Shelf Res 30(3–4):353–364. https://doi.org/10.1016/j.csr.2009.12.003

Bernier NB, Thompson KR (2015) Deterministic and ensemble storm surge prediction for Atlantic Canada with lead times of hours to

ten days. Ocean Model 86:114–127. https://doi.org/10.1016/j.ocemod.2014.12.002

Bitz CM, Lipscomb WH (1999) An energy-conserving thermodynamic model of sea ice. J Geophys Res Oceans 104(C7):148–227. https://doi.org/10.1029/1999JC900100

Bourgault D, Koutitonsky VG (1999) Real-time monitoring of the freshwater discharge at the head of the St. Lawrence Estuary Atmosphere-Ocean 37(2):203–220

Brasnett B (2008) The impact of satellite retrievals in a global sea-surface temperature analysis. Quart J Roy Meteor Soc 134:1745–1760. https://doi.org/10.1002/qj.319

Brasnett B, Surcel-Colan D (2016) Assimilating retrievals of Sea Surface temperature from VIIRS and AMSR2. J Atmos Ocean Technol 33(2):361–375. https://doi.org/10.1175/JTECH-D-15-0093.1

Brickman D, Hebert D, Wang Z (2018) Mechanism for the Recent Ocean Warming Events on the Scotian Shelf of Eastern Canada. Cont Shelf Res 156(1):2018

Buehner M, Caya A, Pogson L, Carrieres T, Pestieau P (2013) A New Environment Canada Regional Ice Analysis System. Atmos Ocean 51(1):18–34

Buehner M, Caya A, Carrieres T, Pogson L (2016) Assimilation of SSMIS and ASCAT data and the replacement of highly uncertain estimates in the Environment Canada Regional Ice Prediction System. Q J Roy Meteor Soc 142(695):562–573

Caron JF (2022) High Resolution Deterministic Prediction System – National Domain (HRDPS-NAT), update from version 5.2.0 to version 6.0.0 https://collaboration.cmc.ec.gc.ca/cmc/cmoi/product_guide/docs/tech_notes/technote_hrdps-600_e.pdf

Carrère L, Lyard F, Cancet M, Guillot A, Roblou L (2012) FES2012: A new global tidal model taking taking advantage of nearly 20 years of altimetry, Proceedings of meeting 20 Years of Altimetry, Venice 2012

Carrieres T, Greenan B, Prinsenberg S, Peterson IK (1996) Comparison of Canadian ice charts with surface observations off Newfoundland, winter 1992. Atmos Ocean 34:207–236

Cirano M, Charria G, De Mey-Frémaux P, Kourafalou VK, Stanev E (2021) Coastal Ocean Forecasting Science supported by GODAE OceanView Coastal oceans and Shelf. https://doi.org/10.1007/s10236-021-01464-x. Seas Task Team (COSS-TT)—Part II Ocean Dynamics,

Côté J, Gravel S, Méthot A, Patoine A, Roch M, Staniforth A (1998) The operational CMC–MRB Global Environmental Multiscale (GEM) model. Part I: design considerations and Formulation. Mon Wea Rev 126:1373–1395. https://doi.org/10.1175/1520-0493(1998)126%3C1373:TOCMGE%3E2.0.CO;2

Coyne J, Cyr F, Donnet S, Galbraith P, Geoffroy M, Hebert D, Layton C, Ratsimandresy A, Snook S, Soontiens N, Walkusz W (2023) Canadian Atlantic Shelf temperature-salinity (CASTS). https://doi.org/10.20383/102.0739. Federated Research Data Repository

Dai A, Trenberth KE (2002) Estimates of freshwater discharge from continents: latitudinal and seasonal variations. J Hydrometeorol 3:660–687

Drakkar Group (2007) Eddy-permitting ocean circulation hindcasts of past decades. CLIVAR Exch 12(3):8–10

Dronkers JJ (1969) Tidal computations for rivers, coastal areas, and seas. Journal of the hydraulics division, Proceedings of the American Society of Civil Engineers, 49

Dupont F, Higginson S, Bourdallé-Badie R, Lu Y, Roy F, Smith G, Lemieux J-F, Garric G, Davidson F (2015) A high-resolution ocean and sea-ice modelling system for the Arctic and North Atlantic oceans. Geosci Model Dev 8(5):1577–1594. https://doi.org/10.5194/gmd-8-1577-2015

Dupont et al (2021) Water Cycle Prediction System (WCPS) version 3.0.0. Technical Note. Canadian Meteorological Center. https://collaboration.cmc.ec.gc.ca/cmc/CMOI/product_guide/docs/tech_notes/technote_wcps-300_e.pdf

Durnford D, Fortin V, Smith GC, Archambault B, Deacu D, Dupont F, Dyck S, Martinez Y, Klyszejko E, MacKay M, Liu L, Pellerin P, Pietroniro A, Roy F, Vu V, Winter B, Yu W, Spence C, Bruxer J, Dickhout J (2018) Toward an operational water cycle prediction system for the Great Lakes and St. Lawrence River. Bull Am Meteorol Soc 99(3):521–546

Egbert GD, Erofeeva SY (2002) Efficient inverse modeling of barotropic ocean tides. J Atmos Ocean Technol 19(2):183–204

Flather R (1976) A tidal model of the Northwest European continental shelf. Mem Soc R Sci Liege 10(6):141–164

Foreman M, Walters R, Henry R, Keller C, Dolling A (1995) A tidal model for eastern Juan De Fuca Strait and the southern Strait of Georgia. J Phys Res 100(C1):721–740

Fringer OB, Dawson CN, He R, Ralston DK, Zhang YJ (2019) The future of coastal and estuarine modeling: findings from a workshop. Oc Mod 143. https://doi.org/10.1016/j.ocemod.2019.101458

García Sotillo M, Cailleau S, Aznar R, Aouf L, Barrera E et al (2021) The Operational CMEMS IBI-MFC Service Today: Review of Major Achievements along the Copernicus-1 Service Phase (2015–2021). 9th EuroGOOS International conference, Shom; Ifremer; EuroGOOS AISBL, May 2021, Brest, France. pp.321–328. ffhal-03336265v2f

Garrett CJ, Keeley JR, Greenberg DA (1978) Tidal mixing versus thermal stratification in the Bay of Fundy and Gulf of Maine. Atmos–Ocean 16:403–423. https://doi.org/10.1080/07055900.1978.9649046

Gasset N (2019) Global Deterministic Prediction System (GDPS), update from version 6.1.0 to version 7.0.0. https://collaboration.cmc.ec.gc.ca/cmc/cmoi/product_guide/docs/tech_specifications/tech_specifications_GDPS_e.pdf

Hirose N, Usui N, Sakamoto K, Tsujino H, Yamanaka G, Nakano H, Urakawa S, Toyoda T, Fujii Y, Kohna N (2019) Development of a new operational system for monitoring and forecasting coastal and open-ocean states around Japan. Ocean Dyn 69:1333–1357. https://doi.org/10.1007/s10236-019-01306-x

Hunke EC (2001) Viscous-plastic sea ice dynamics with the EVP model: linearization issues. J Comput Phys 170:18–38

Hunke EC, Lipscomb WH (2008) CICE: the Los Alamos sea ice model. Documentation and software user's manual version 4.0 (tech. Rep. LA-CC-06-012). Los Alamos National Laboratory, Los Alamos, NM

Janeković I, Powell B (2011) Analysis of imposing tidal dynamics to nested numerical models. Cont Shelf Res 34:30–40. https://doi.org/10.1016/j.csr.2011.11.017

Katavouta A, Thompson KR, Lu Y, Loder JW (2016) Interaction between the tidal and seasonal variability of the Gulf of Maine and Scotian Shelf region. J Phys Oceanogr 46(11):3279–3298. https://doi.org/10.1175/JPO-D-15-0091.1

Kourafalou VH, De Mey P, Le Hénaff M, Charria G, Edwards CA, He R, Herzfeld M, Pascual A, Stanev EV, Tintoré J, Usui N, van der Westhuysen AJ, Wilkin J, Zhu X (2015a) Coastal Ocean forecasting: system integration and evaluation. J Oper Oceanogr 8:sup1

Kourafalou VH, De Mey P, Staneva J, Ayoub N, Barth A, Chao Y, Cirano M, Fiechter J, Herzfeld M, Kurapov A, Moore AM, Oddo P, Pullen J, van der Westhuysen A, Weisberg RH (2015b) Coastal Ocean forecasting: science foundation and user benefits. J Oper Oceanogr 8:sup1 s147-167. https://doi.org/10.1080/1755876X.2015.1022348

Koutitonsky VG, Bugden GL (1991) The physical oceanography of the Gulf of St. Lawrence: A review with emphasis on the synoptic variability of the motion, in The Gulf of St. Lawrence: Small Ocean or Big Estuary? edited by J.-C. Therriault, Can. Spec. Publ. Fish. Aquat.Sci., 113, 57– 90

Kurapov AL, Erofeeva SY, Myers E (2017) Coastal sea level variability in the US West Coast Ocean forecast system (WCOFS). Ocean Dyn 67(1):23–36. https://doi.org/10.1007/s10236-016-1013-4

Large WG, Yeager S (2004) Diurnal to decadal global forcing for ocean and sea-ice models: The data sets and flux climatologies (No. NCAR/TN-460 + STR). University Corporation for Atmospheric Research. https://doi.org/10.5065/D6KK98Q6

Lefaivre D, D'Astous A, Matte (2016) Hindcast of Water Level and Flow in the St. Lawrence River over the 2005–2012 period. Atmos Ocean. https://doi.org/10.1080/07055900.2016.1168281

Lemieux J-F, Tremblay LB, Dupont F, Plante M, Smith GC, Dumont D (2015) A basal stress parameterization for modeling landfast ice. J Geophys Res 120(4):3157–3173. https://doi.org/10.1002/2014JC010678

Lemieux J-F, Dupont F, Blain P, Roy F, Smith GC, Flato GM (2016) Improving the simulation of landfast ice by 815 combining tensile strength and a parameterization for grounded ridges. J Geophys Res 121(10):7354–7368

Levier B, Treguier A-M, Madec G, Garnier V (2007) Free surface and variable volume in the nemo code. Tech. rep., MERSEA MERSEA IP report WP09-CNRS-STR-03-1A, 47pp, available on the NEMO web site

Lipscomb WH, Hunke EC, Maslowski W, Jakacki J (2007) Ridging, strength, and stability in high-resolution sea ice models. J Geophys Res 112(C03S91). https://doi.org/10.1029/2005JC003355

Lorente P, Sotillo M, Amo-Baladrón A, Aznar R, Levier B, Sánchez-Garrido JC, Sammartino S, de Pascual-Collar Á, Reffray G, Toledano C, Álvarez-Fanjul E (2019b) Skill assessment of global, regional, and coastal circulation forecast models: evaluating the benefits of dynamical downscaling in IBI (Iberia–Biscay–Ireland) surface waters. Ocean Sci 15:967–996. https://doi.org/10.5194/os-15-967-2019

Madec G, Imbard M (1996) A global ocean mesh to overcome the North Pole singularity. Clim Dyn 12:381–388

Madec G et al (2015) NEMO ocean engine, note Du Pole De modélisation. France. Ver 3.6 stable. ISSN No 1288–1619

Maraldi C, Chanut J, Levier B, Ayoub NK, De Mey P, Reffray G, Lyard FH, Cailleau S, Drévillon M, Álvarez Fanjul E, Sotillo MG, Marsaleix P (2013) NEMO on the shelf: assessment of the Iberia-Biscay-Ireland configuration. Ocean Sci 9(2013):745–771

Mellor G, Blumberg A (2004) Wave breaking and Ocean Surface Layer Thermal Response. J Phys Oceanogr 34(3):693–698

Milbrandt JA, Bélair S, Faucher M, Vallée M, Carrera ML, Glazer A (2016) The pan-canadian high resolution (2.5 km) deterministic prediction system. Weather Forecast 31(6):1791–1816. https://doi.org/10.1175/WAF-D-16-0035.1

Nudds S, Lu Y, Higginson S, Haigh SP, Paquin J-P, O'Flaherty-Sproul M, Taylor S, Blanken H, Marcotte G, Smith GC, Bernier NB, MacAulay P, Wu Y, Zhai L, Hu X, Chanut J, Dunphy M, Dupont F, Greenberg D, Davidson FJM, Page F (2020) Evaluation of structured and unstructured models for application in operational ocean forecasting in Nearshore Waters. J Mar Sci Eng 8(7):484. https://doi.org/10.3390/jmse8070484

Paquin J-P, Lu Y, Taylor S, Blanken H, Marcotte G, Hu X, Zhai L, Higginson S, Nudds S, Chanut J, Smith GC, Bernier N, Dupont F (2019) High-resolution modelling of a coastal harbour in the presence of strong tides and significant river runoff. Ocean Dyn 70:365–385. https://doi.org/10.1007/s10236-019-01334-7

Paquin J-P, Roy F, Smith GC, Dupont F, MacDermid S, Hata Y, Huizy O, Lei J, Martinez Y, Blanken H, Holden J, Soontiens N (2021a) Coastal Ice Ocean Prediction System for the East Coast of Canada (CIOPS-E) – Update from version 1.5.0 to 2.0.0. *Canadian Centre for Meteorological and Environmental Prediction Technical Note* December 1st 2021. [https://collaboration.cmc.ec.gc.ca/cmc/CMOI/product_guide/docs/tech_notes/technote_ciops-east-200_e.pdf]

Paquin J-P, Smith GC, Dupont F, MacDermid S, Haha Y, Huizy O, Lei J, Martinez Y, Dunphy M, Krassovski M, Taylor S, Blanken H, Holden J, Soontiens N, Allen SE, Latornell D (2021b) Coastal Ice Ocean Prediction System for the West Coast of Canada (CIOPS-W) – Update from version 1.5.0 to 2.0.0. *Canadian Centre for Meteorological and Environmental Prediction Technical Note* December 1st 2021. [https://collaboration.cmc.ec.gc.ca/cmc/CMOI/product_guide/docs/tech_notes/technote_ciops-west-200_e.pdf]

Paquin J-P, Roy F, Smith GC, Dupont F, MacDermid S, Hata Y, Huizy O, Lei J, Lu Y, Taylor S, Blanken H (2022a) Coastal Ice Ocean Prediction System for the East Coast of Canada (CIOPS-E) – System description for version 1. *Canadian Centre for Meteorological and Environmental Prediction Technical Note*. April 20th 2022. [https://collaboration.cmc.ec.gc.ca/cmc/CMOI/product_guide/docs/tech_notes/technote_ciops-east-100_e.pdf]

Paquin J-P, Smith GC, Roy F, Dupont F, MacDermid S, Lei J, Lu Y, Taylor S, Blanken H, Zhai L (2022b) Coastal Ice Ocean Prediction System for the West Coast of Canada (CIOPS-W) – System description for version 1.0.0 and 1.5.0. *Canadian Centre for Meteorological and Environmental Prediction Technical Note*. April 27th 2021. [https://collaboration.cmc.ec.gc.ca/cmc/CMOI/product_guide/docs/tech_notes/technote_ciops-west-100_e.pdf]

Pawlowicz R, Beardsley B, Lentz S (2002) Classical tidal harmonic analysis including error estimates in MATLAB using T TIDE. Comput Geosci 28(8):929–937

Pellerin P, Ritchie H, Saucier FJ, Roy F, Desjardins S, Valin M, Lee V (2004) Impact of a two-way coupling between an Atmospheric and an ocean-ice model over the Gulf of St. Lawrence. Mon Weather Rev 132(6):1379–1398

Rascle N, Ardhuin F, Queffeulou P, Croizé-Fillon D (2008) A global wave parameter database for geophysical applications. Part 1: Wave-current–turbulence interaction parameters for the open ocean based on traditional parameterizations. Ocean Model 25(Issues 3–4):154–171. https://doi.org/10.1016/j.ocemod.2008.07.006

Reszka MK, Swaters GE (1999) Numerical investigation of baroclinic instability in the Gaspé Current using a frontal geostrophic model. J Geophys Research: Oceans 104(C11):25685–25696

Roy F, Bélanger J-M, Dyck S, Dupont F, Lemieux J-F, Beaudoin C, Chanut J, Garric G, Pellerin P, Ritchie H, Lu Y, Davidson F (2014) Update of the Regional Marine Prediction System – Gulf of St. Lawrence (RMPS-GLS) with NEMO-CICE. *Canadian Centre for Meteorological and Environmental Prediction Technical Note* December 1st 2021. [https://collaboration.cmc.ec.gc.ca/cmc/cmoi/product_guide/docs/lib/technote_rmps-gsl-600_20141118_e.pdf]

Roy F, Chevallier M, Smith GC, Dupont F, Garric G, Lemieux J-F, Lu Y, Davidson F (2015) Arctic sea ice and freshwater sensitivity to the treatment of the atmosphere-ice-ocean surface layer. J Geophys Res - Oceans, 120(6), 4392 – 880 4417

Sakamoto K, Yamanaka G, Tsujino H, Nakano H, Urakawa S, Usui N, Hirabara M, Ogawa K (2016) Development of an operational coastal model of the Seto Inland Sea, Japan. Ocean Dyn 66:77–97. https://doi.org/10.1007/s10236-015-0908-9

Sakamoto K, Tsujino H, Nakano H, Urakawa S, Toyoda T, Hirose N, Usui N, Yamanaka G (2019) Development of a 2-km resolution ocean model covering the coastal seas around Japan for operational application. Ocean Dyn 69:1181–1202. https://doi.org/10.1007/s10236-019-01291-1

Saucier FJ, Chassé J (2000) Tidal circulation and buoyancy effects in the St. Lawrence Estuary. Atmos Ocean 38(4):505–556

Saucier FJ, Roy F, Gilbert D, Pellerin P, Ritchie H (2003) Modeling the formation and circulation processes of water masses and sea ice in the Gulf of St. Lawrence, Canada. J Geophys Res 108:3269. https://doi.org/10.1029/2000JC000686

Saucier FJ, Roy F, Senneville S, Smith G, Lefaivre D, Zakardjian B, Dumais J-F (2009) Modélisation de la circulation dans L'estuaire et le golfe du Saint-Laurent en réponse aux variations du débit d'eau douce et des vents. Revue des sciences de L'eau /. J Water Sci 22(2):159–176. https://doi.org/10.7202/037480ar

Shchepetkin AF, McWilliams JC (2005) The regional oceanic modeling system (roms) - a split-explicit, free-surface, topography-following-coordinate oceanic modelr. Ocean Model 9(4):347–404

Sheng J (2001) Dynamics of a buoyancy-driven Coastal Jet: the Gaspé Curreny. J Phys Oceanogr 31:11: 3146–3162. https://doi.org/10.1175/1520-0485(2001)031%3C3146:DOABDC%3E2.0.CO;2

Smagorinsky J (1993) In: Galperin B, Orszag SA (eds) Large Eddy Simulation of Complex Engineering and Geophysical flows, chap. Some historical remarks on the use of non-linear viscosities. Cambridge University Press, pp 3–36

Smith GC, Fortin AS (2022) Verification of Eddy properties in operational oceanographic analysis systems, vol 172. Ocean Modelling, p 101982

Smith SD, Anderson RJ, Oost WA, Kraan C, Katsaros KB, Davidson KL, Bumke K, Hasse L, Chadwick HM (1992) Sea surface wind stress and drag coefficients: the hexos results. Boundary-Layer Meteorol 60:109–142. https://doi.org/10.1007/BF00122064

Smith GC, Saucier FJ, Straub D (2006a) Formation and circulation of the cold intermediate layer in the Gulf of Saint Lawrence. J Geophys Res 111:C06011. https://doi.org/10.1029/2005JC003017

Smith GC, Saucier FJ, Straub D (2006b) Response of the lower St. Lawrence Estuary to external forcing in winter. J Phys Oceanogr 36(8):1485–1501. https://doi.org/10.1175/JPO2927.1

Smith GC, Roy F, Brasnett B (2013) Evaluation of an operational ice–ocean analysis and forecasting system for the Gulf of St Lawrence. Q J R Meteorol Soc 139(671):419–433

Smith GC, Bélanger JM, Roy F, Pellerin P, Ritchie H, Onu K, Roch M, Zadra A, Surcel-Colan D, Winter B, Fontecilla JS, Deacu D (2018) Impact of coupling with an ice–ocean model on global medium-range NWP Forecast Skill. Mon Weather Rev 146(4):1157–1180

Smith GC, Liu Y, Benkiran M, Chikhar K, Surcel-Colan D, Gauthier AA, Testut CE, Dupont F, Lei J, Roy F, Lemieux JF (2021) The Regional Ice Ocean Prediction System v2: a pan-canadian ocean analysis system using an online tidal harmonic analysis. Geosci Model Dev 14(3):1445–1467

Soontiens N, Allen SE, Latornell D, Le Souëf K, Machuca I, Paquin J-P, Lu Y, Thompson K, Korabel V (2016) Storm surges in the Strait of Georgia simulated with a Regional Model. Atmos Ocean 54(1):1–21. https://doi.org/10.1080/07055900.2015.1108899

Thompson KR, Sheng JY, Smith PC, Cong LZ (2003) Prediction of surface currents and drifter trajectories on the inner Scotian shelf. J Geophys Research-Oceans 108:3287. https://doi.org/10.1029/2001JC001119

Thompson KR, Wright DG, Lu Y, Demirov E (2006) A simple method for reducing seasonal bias and drift in eddy resolving ocean models. Ocean Modell 13(2):109–125

Tonani M, Sykes P, King RR, McConnell N, Péquignet A-C, O'Dea E, Graham JA, Polton J, Siddorn J (2019) The impact of a new high-resolution ocean model on the Met Office North-West European Shelf forecasting system. Ocean Sci 15:1133–1158. https://doi.org/10.5194/os-15-1133-2019

Trotta F, Fenu E, Pinardi N, Bruciaferri D, Giacomelli L, Federico I, Gi C (2016) A structured and unstructured grid relocatable ocean platform for forecasting (SURF). Deep Sea Res II Top Stud Oceanogr 133:54–75

Trotta F, Pinardi N, Fenu E, Grandi A, Lyubartsev V (2017) Multi-nest high-resolution model of submesoscale circulation features in the Gulf of Taranto. Ocean Dyn 67(12):1609–1625. https://doi.org/10.1007/s10236-017-1110-z

Umlauf L, Burchard H (2003) A generic length-scale equation for geophysical turbulence models. J Mar Res 61(2):235–265

Vignudelli S, Birol F, Benveniste J, Fu LL, Picot N, Raynal M, Roinard H (2019) Satellite altimetry measurements of sea level in the coastal zone. Surv Geophys 40:1319–1349